Complex potential well

a research training report by Max Lewandowski

July 26, 2011

Supervisor: Priv.-Doz. Dr. Axel Pelster

Contents

1 Introduction

Already in 1924 Satyendranath Bose wrote a paper where he used a novel way for counting states of identical photons to derive Planck's quantum radiation law. In this way he found out that the Maxwell-Boltzmann distribution is not true for microscopic particles and has to be replaced by another distribution [1]. In the same year this idea was extended to massive particles by Albert Einstein [2], therefore this new distribution is called *Bose-Einstein distribution*. It predicts a macroscopic occupation of the ground state by a dense collection of particles with integer spin, called bosons, for very low temperatures near to absolute zero. This phenomenon is called *Bose-Einstein condensation*. The first experimental realization of a pure Bose-Einstein condensate (BEC) was accomplished in 1995 by Eric Cornell and Carl Wieman at JILA [3] and Wolfgang Ketterle at MIT [4]. The creation of a BEC requires temperatures very near absolute zero to reach the critical temperature for the phase transition. The new techniques of laser cooling [5–7] and magnetic evaporative cooling [8] made it possible for E. Cornell and C. Wiedman to cool down a gas of rubidium-87 atoms confined in a magnetic time-averaged, orbital potential (TOP) trap to 170 nanoKelvin which undermatches the critical temperature of ^{87}Rb. In the same year W. Ketterle produced at MIT a much larger BEC of sodium-23, which allowed him to observe even first coherence effects like the quantum mechanical interference between two different BECs [9].

So far BECs have been created with many other kinds of atoms like ^{1}H, ^{7}Li, ^{23}Na, ^{39}K, ^{41}K, ^{52}Cr, ^{85}Rb, ^{87}Rb, ^{133}Cs, ^{170}Yb, ^{174}Yb and ^{4}He in an excited state. Moreover, experiments with BEC as well as its theory became one of the most interesting physical research topics in the last years like the realization of a BEC in optical lattices which are standing laser fields that yield via the AC Stark effect periodic potential wells for atoms [10, 11]. This leads to a strongly correlated BEC which is well controlled by the respective laser parameters and yields for increasing laser intensities a quantum phase transition from the superfluid to a Mott phase. As the latter is characterized by a fixed number of bosons in each well, a Bose gas in an optical lattice is a promising candidate for quantum simulations like entanglement of atoms or quantum teleportation [12]. Also disordered Bose gases can be realized via laser speckles or incommensurable optical lattices to create random potentials [13]. Another interesting research field are fermionic condensates. Two weakly correlated fermions called *Cooper pairs* yield a "particle" with integer spin which therefore also obeys Bose-Einstein statistics despite the fermionic constituents. By increasing the correlation for example by a magnetic trap there is a phase transition from this BCS phase of weakly coupled fermions [14] to bound boson molecules condensing to a BEC, which is called BCS-BEC-crossover [15].
Furthermore, complex potentials are used in a BEC as a heuristic tool to model dissipation processes which occur once a BEC is brought in contact, for instance, with an ion [18]. This research work is related to an experiment performed by Herwig Ott [16, 17] from the Technical University of Kaiserslautern where a Rb^{87}-BEC interacts with an electron beam according to Fig. 1, which is one technique to achieve single-site adressabilities [19–22].

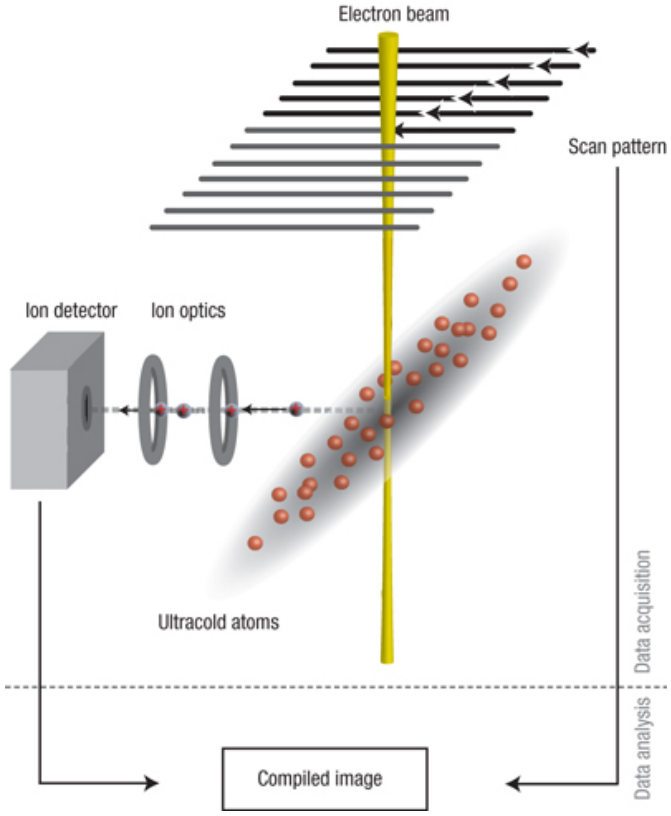

Figure 1: The atomic ensemble is prepared in an optical dipole trap. An electron beam with variable beam current and diameter is scanned across the cloud. Electron impact ionization produces ions, which are guided with an ion optical system towards a channeltron detector. The ion signal together with the scan pattern is used to compile the image [17].

The BEC is confined by an anisotropic harmonic trap with the frequencies $\omega_\perp = 2\pi \cdot 13$ Hz and $\omega_{||} = 2\pi \cdot 170$ Hz and contains about 100 000 atoms. The experiment was realized at about 80 nK, the critical temperature of ^{87}Rb is 300 nK. The current density caused by the electron beam has the form of a Gaussian beam

$$j(x,y) = \frac{\sigma_{\text{tot}}}{e}\frac{I}{2\pi w^2}\exp\left[-\frac{(r-r_0)^2}{2w^2}\right], \tag{1.1}$$

where $\sigma_{\text{tot}} = 1.7 \cdot 10^{-20}$ m^2 denotes the total cross section of the ^{87}Rb-atoms, $I = 20$ nA is the electron current and the waist of the beam is denoted by $w = (8\ln 2)^{-1/2} \cdot \text{FWHM}$, where FWHM yields the full width at half maximum, which is about 100 nm $-$ 500 nm. The beam is directed in z-direction so that $(r-r_0)^2 = (x-x_0)^2 + (y-y_0)^2$. In contrast to the other applications of complex potentials the experimental setup of Herwig Ott makes it possible to control all experimental parameters to a high degree. Therefore, this electron beam technique seems to be the most promising candidate to compare the respective experimental results with theoretical calculations in a quantitive way. We are now interested in the interaction of the BEC with the beam. The main idea is to model this interaction by an imaginary potential with a width given by the Gaussian profile of the beam. The whole BEC is confined in a harmonic trap which is modelled by a real potential.
In this research work we aim at getting a fundamental view on the theory of the properties and

effects of a BEC in a complex potential $V(\boldsymbol{x}) = V_R(\boldsymbol{x}) + iV_I(\boldsymbol{x})$ at absolute zero which is described by the Gross-Pitaevskii equation

$$i\hbar\frac{\partial}{\partial t}\psi(\boldsymbol{x},t) = \left[-\frac{\hbar^2}{2M}\Delta + V(\boldsymbol{x}) + g\left|\psi(\boldsymbol{x},t)\right|^2\right]\psi(\boldsymbol{x},t). \tag{1.2}$$

Here ψ represents the wave function of the condensate, V_R stands for the harmonic trap, V_I is proportional to the Gaussian beam (1.1) and g describes the two-particle interaction. Eq. (1.2) represents a 3-dimensional nonlinear partial differential equation for ψ. As we aim here at getting a fundamental look at a BEC in a complex potential, we start with simplifying this problem. First we consider a model in only one spatial dimension. Furthermore, we approximate both potentials V_R and V_I by square well potentials. Thus our model system consists of two nested square well potentials where the inner one is imaginary with the width equal to the diameter of the beam $2w$ and the outside one is real with a width equal to the spatial extension of the BEC, which we denote by $2L$. Moreover, we neglect interactions between ^{87}Rb-atoms which can be experimentally performed by using magnetic traps and taking advantage of hyperfine structures. In this way it is possible to influence scattering parameters like the cross section and the scattering length via magnetic Feshbach resonances [23], which are induced by the additional magnetic field. It is thus possible to manage a vanishing scattering length and cross section, that is a vanishing interaction. With these simplifications each particle of the BEC can be seperatly described by a one-dimensional linear Gross-Pitaevskii equation which is just a Schrödinger equation.
In Chapter 2 we start with a general theoretical approach to the Schrödinger equation with a complex potential, considering the corresponding states and their dynamics, the continuity equation, quantization conditions and end up for consistency with the evaluation of the real limit. In Chapter 3 we plot and discuss the energies, densities and currents of the complex potential well and discuss some interesting issues occuring in Chapter 2. All this is then concluded by a general outlook on possible improvements and further research in this topic in Chapter 4.

2 Complex 1-dimensional square well potential

We consider the one-dimensional time-dependent Schrödinger equation

$$i\hbar\frac{\partial}{\partial t}\psi(x,t) = H\psi(x,t), \tag{2.1}$$

where H denotes the Hamilton operator

$$H = -\frac{\hbar^2}{2M}\frac{\partial^2}{\partial x^2} + V(x) \tag{2.2}$$

with a complex potential $V(x) := V_R(x) + iV_I(x)$. The real and imaginary part are given by

$$V_R(x) := \begin{cases} 0 & , \ |x| < L \\ \infty & , \ \text{otherwise} \end{cases} \quad \text{and} \quad V_I(x) := \begin{cases} -C = \text{const.} & , \ |x| < w < L \\ 0 & , \ \text{otherwise} \end{cases}, \tag{2.3}$$

where $C > 0$. We call the interval $-L \leq x \leq -w$ "area 1" and $-w \leq x \leq +w$ "area 2" which is followed by "area 3" $w \leq x \leq L$.

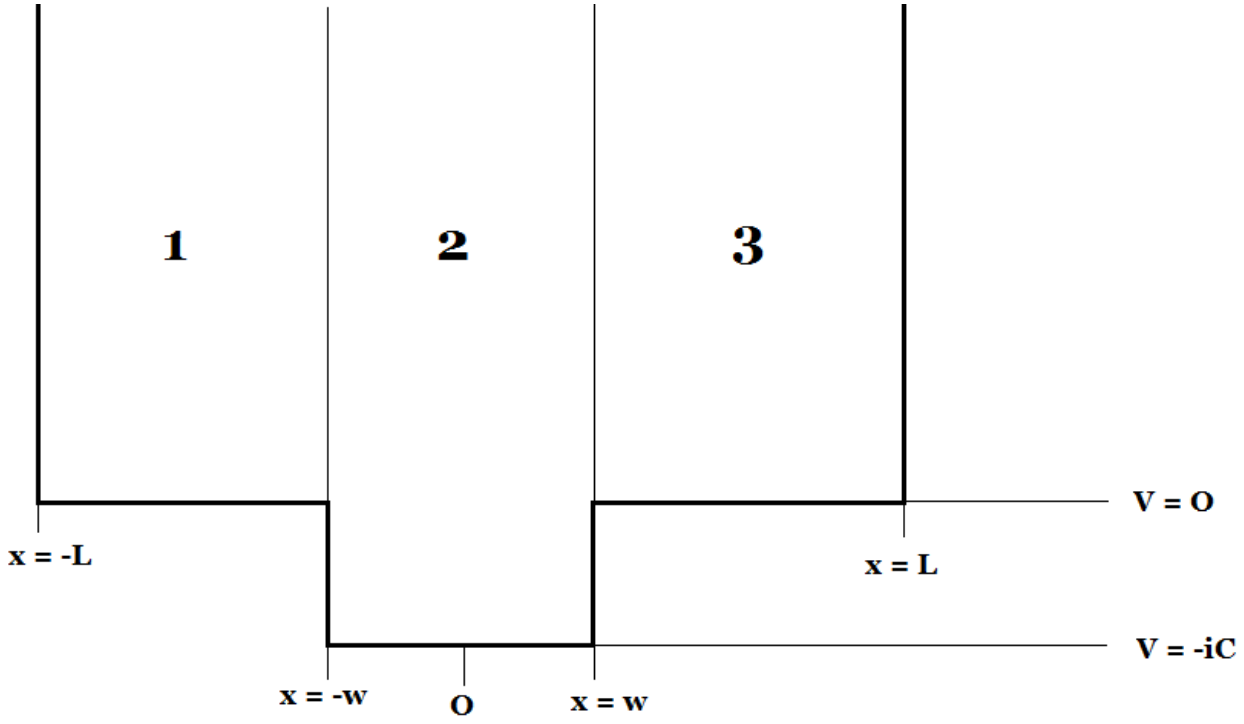

Figure 2: Schematic sketch of the complex potential well.

2.1 Schrödinger equation

The time-dependent Schrödinger equation (2.1) governs the time evolution of the system. A formal solution of this differential equation is of the form

$$\psi(x,t) = U(t,t_0)\psi(x,t_0), \tag{2.4}$$

where $U(t,t_0)$ denotes the time evolution operator. Inserting this solution into (2.1) yields that $U(t,t_0)$ has to fullfill the Schrödinger equation

$$i\hbar\frac{\partial}{\partial t}U(t,t_0) = HU(t,t_0). \tag{2.5}$$

If the Hamilton operator H does not depend on time, i.e. it commutes with itself for distinct times $t \neq t_0$, we can immediatly integrate (2.5) and obtain

$$U(t,t_0) = \exp\left[-\frac{i}{\hbar}H(t-t_0)\right]. \tag{2.6}$$

If additionally $\psi(x,t_0)$ is an eigenvector of H and the energy E the corresponding eigenvalue, the formal solution (2.4) of the time-dependent Schrödinger equation becomes

$$\psi(x,t) = \psi(x,t_0)\exp\left[-\frac{i}{\hbar}E(t-t_0)\right]. \tag{2.7}$$

For the familiar potential well of a real potential with the corresponding time-independent and hermitian Hamilton operator the solution (2.7) represents a stationary state. Stationarity means that the absolute square of this state does not depend on time, that is for arbitrary times t:

$$\psi^*_{\text{stat}}(x,t)\psi_{\text{stat}}(x,t) = \psi^*_{\text{stat}}(x,t_0)\psi_{\text{stat}}(x,t_0) \quad \Rightarrow \quad \rho_{\text{stat}}(x,t) = \rho_{\text{stat}}(x,t_0), \tag{2.8}$$

where $\rho(x,t) = \psi^*(x,t)\psi(x,t)$ denotes the probability density, which is a physical measurable quantity in contrast to ψ. Stationarity of the wavefunction is obviously ensured by real energies E in (2.7).
Generalizing all this to a complex potential is directly followed by a non-hermitian Hamiltonian so that we have to deal with complex energy eigenvalues. The time evolution operator (2.6) is thus not unitary because H is not hermitian. Therefore, the probability density $\rho = \psi^*\psi$ of a solution of (2.7) evolves exponentially with the imaginary part E_I of the energy:

$$\rho(x,t) = \exp\left[\frac{2}{\hbar}E_I(t-t_0)\right]\rho(x,t_0). \tag{2.9}$$

This disagrees to the stationarity condition (2.8) so that for a complex potential the eigenstates of H are not stationary any more. Consistently this is only fullfilled for $E_I = 0$, that is the familiar real potential well. Otherwise one can differ between $E_I > 0$ and $E_I < 0$. While for $E_I > 0$ the probability density is increased by the complex potential, the case of $E_I < 0$ yields a damping effect that is ρ decreases with time because of the complexity of the potential.

2.2 Continuity equation

The familiar approach to derive the continuity equation is to multiply the time-dependent Schrödinger equation with the complex conjugated wavefunction $\psi^*(x,t)$ as well as the complex conjugated one with $\psi(x,t)$ and add both expressions:

$$\begin{aligned}\psi^*(x,t)\frac{\partial}{\partial t}\psi(x,t) + \psi(x,t)\frac{\partial}{\partial t}\psi^*(x,t) &= \frac{\partial}{\partial t}\left[\psi^*(x,t)\psi(x,t)\right] \\ &= \frac{i}{\hbar}\left[\psi(x,t)H^\dagger\psi^*(x,t) - \psi^*(x,t)H\psi(x,t)\right],\end{aligned} \tag{2.10}$$

where H denotes the Hamilton operator, which is not hermitian for $V_I \neq 0$. The left-hand side of the equation yields the time derivative of the probability density

$$\rho(x,t) = \psi^*(x,t)\psi(x,t), \tag{2.11}$$

while the sum of the kinetic parts

$$-\frac{i}{\hbar}\left[\psi(x,t)\frac{\hbar^2}{2M}\frac{\partial^2}{\partial x^2}\psi^*(x,t)-\psi^*(x,t)\frac{\hbar^2}{2M}\frac{\partial^2}{\partial x^2}\psi(x,t)\right] \tag{2.12}$$

on the right-hand side, which is hermitian, is commonly interpreted as the negative divergence of some *probability current*

$$\begin{aligned} j(x,t) &= \frac{i\hbar}{2M}\left[\psi(x,t)\frac{\partial}{\partial x}\psi^*(x,t)-\psi^*(x,t)\frac{\partial}{\partial x}\psi(x,t)\right] \\ &= \frac{\hbar}{M}\mathrm{Im}\left[\psi^*(x,t)\frac{\partial}{\partial x}\psi(x,t)\right], \end{aligned} \tag{2.13}$$

which is a real quantity. One can see directly from the definitions that $\rho(x,t)$ is always a spatial symmetric function because the wavefunction as well as its complex conjugated has to be either symmetric or antisymmetric for our chosen symmetric potential since the Hamiltonian (2.2) is symmetric and the product of two functions with definite parity is always symmetric. In contrast to this the current $j(x,t)$ is always antisymmetric in x because the derivative of a function with a defined parity always has the opposite parity. Therefore, the product of such a function and its derivative is always antisymmetric.

Now let us come to the continuity equation. If there were no potential the change of $\rho(x,t)$ with time would formally be only caused by the source density of j so that we are left with the continuity equation like there are no "sources" and "drains" present:

$$\frac{\partial}{\partial t}\rho(x,t)+\frac{\partial}{\partial x}j(x,t)=0. \tag{2.14}$$

Such terms will occur on the right-hand side of (2.14) if H contains a potential V with a non-vanishing imaginary part V_I so that in Eq. (2.12) the imaginary parts add up and there remains a term proportional to $V_I(x)\rho(x,t)$ in addition to the derivative $\frac{\partial}{\partial x}j(x,t)$, whereas the real part V_R cancels. Therefore, only the imaginary part of the potential V_I plays the role of a "drain of probability", that could be interpreted as a kind of dissipation in a system with many particles. Therefore, in area 2, where $V_I \neq 0$, we will get a contribution on the right-hand side of (2.14):

$$\frac{\partial}{\partial t}\rho(x,t)+\frac{\partial}{\partial x}j(x,t)=\frac{2}{\hbar}V_I(x)\rho(x,t). \tag{2.15}$$

This expression contains an interesting insight. Here ρ is a continuous and differentiable function on the interval $(-L,L)$ because it consists of the product of two functions with these properties. Therefore, $\frac{\partial\rho}{\partial t}$ is continuous, too. The right-hand side of (2.15) is obviously not continuous at $x=\pm w$, which can directly be seen from the definition of V_I in (2.3). Thus, we can conclude that then also $\frac{\partial j}{\partial x}$ must also have discontinuities there. Thus the probability current $j(x,t)$ is not differentiable at $x=\pm w$.

2.3 Static solutions

Since we know the time evolution for our time-independent Hamiltonian, let us now discuss solutions of the remaining static part. Therefore, we have to solve the time-independent Schrödinger equation

$$H\psi(x) = E\psi(x), \tag{2.16}$$

which is nothing else than the eigenvalue equation of H and we have to find the eigenvalues E and the eigenstates $\psi(x)$, which are in general complex. For this we have to solve (2.16) with the corresponding Hamilton operator (2.2), which is formally equivalent to the classical equation of motion of a harmonic oscillator. In the outer region of the well, i.e. $|x| > L$, the wavefunction vanishes because the probabibilty of the particle to be out of the box is supposed to be equal to zero. In the inner region we have formally to distinguish between the three areas. Therefore, the resulting total wavefunction should have the following form:

$$\psi(x) = \begin{cases} \psi_1(x), & -L \leq x \leq -w \\ \psi_2(x), & -w \leq x < w \\ \psi_3(x), & w \leq x < L \\ 0, & |x| > L \end{cases} . \tag{2.17}$$

As the Hamiltonian (2.2) is isotropic for the complex potential (2.3), the total wavefunction should have a definite parity with respect to the center of the well, which is $x = 0$. This means we assume ψ to be completely symmetric or antisymmetric with respect to $x = 0$. Symmetry of ψ means

$$\psi_1^s(-x) = \psi_3^s(x) \quad \text{and} \quad \psi_2^s(x) = \psi_2^s(-x), \tag{2.18}$$

while in the antisymmetric case ψ fullfills

$$\psi_1^a(-x) = -\psi_3^a(x) \quad \text{and} \quad \psi_2^a(-x) = -\psi_2^a(x) \tag{2.19}$$

in the corresponding areas. This shows that we only have to solve the Schrödinger equation in two different areas because ψ_3 is determined by ψ_1 via symmetry arguments. For area 1 and 2 we make the following general ansatz:

$$\psi_{1,2}(x) = A_{1,2}e^{-ik_{1,2}x} + B_{1,2}e^{ik_{1,2}x}. \tag{2.20}$$

If we insert this into the time-independent Schrödinger equation (2.1) with the respective potentials (2.3), we obtain for the two complex wave-vectors k_1 and k_2:

$$k_1^2 = \frac{2M}{\hbar^2}\left(E_R + iE_I\right) \quad , \qquad k_2^2 = \frac{2M}{\hbar^2}\left[E_R + i(E_I + C)\right]. \tag{2.21}$$

Now we adapt (2.20) to get a respective solution of our problem. Therefore, we use some continuity conditions which arise from the Schrödinger equation (2.1) with the given potential (2.3). It tells us, that due to the box potential V_R the second derivative of the wavefunction $\psi(x)$ is not continuous at $x = \pm L$ so that the first derivative is not differentiable at these points. Because the wavefunction is equal to zero outside of the well, that is $|x| > L$, we take for the continuity of the wavefunction Dirichlet boundary conditions:

$$\psi_1(-L) = A_1 e^{ik_1 L} + B_1 e^{-ik_1 L} = 0 \quad \Leftrightarrow \quad B_1 = -A_1 e^{2ik_1 L}. \tag{2.22}$$

This provides:

$$\psi_1(x) = A_1 \left(e^{-ik_1 x} - e^{2ik_1 L} e^{ik_1 x}\right) = -2iA_1 e^{ik_1 L} \sin\left[k_1(x + L)\right]. \tag{2.23}$$

Thus it follows for ψ_3:

$$\psi_3(x) = \pm\psi_1(-x) = \pm A_1 \left(e^{ik_1 x} - e^{2ik_1 L} e^{-ik_1 x}\right) = \pm 2iA_1 e^{ik_1 L} \sin\left[k_1(x - L)\right] \tag{2.24}$$

depending on the corresponding parity of ψ.
For ψ_2 we can use already the symmetry argument as a condition that has to be fullfilled and therefore eliminate one constant:

$$\psi_2(x) = \pm\psi_2(-x) \quad \Leftrightarrow \quad A_2 e^{-ik_2 x} + B_2 e^{ik_2 x} = \pm\left(A_2 e^{ik_2 x} + B_2 e^{-ik_2 x}\right). \tag{2.25}$$

It follows $A_2 = \pm B_2$ depending on the respective parity of ψ:

$$\psi_2(x) = A_2 \left(e^{-ik_2 x} \pm e^{ik_2 x}\right) \quad \Rightarrow \quad \begin{cases} \psi_2^s(x) & = 2A_2^s \cos k_2^s x \\ \\ \psi_2^a(x) & = -2iA_2^a \sin k_2^a x \end{cases}. \tag{2.26}$$

Even if the potential is only piecewise continuous, ψ has to be continuous and differentiable at $x = -w$ so that

$$\psi_1(-w) = \psi_2(-w) \ , \qquad \frac{\partial}{\partial x}\psi_1(x)\bigg|_{x=-w} = \frac{\partial}{\partial x}\psi_2(x)\bigg|_{x=-w}. \tag{2.27}$$

One can justify this by assuming that ψ and $\frac{\partial}{\partial x}\psi$ are not continuous at $x = -w$. Then a behaviour $\psi(x) \sim \Theta(x + w)$ would imply $\frac{\partial^2}{\partial x^2}\psi(x) \sim \frac{\partial}{\partial x}\delta(x + w)$ as well as $\frac{\partial}{\partial x}\psi(x) \sim \Theta(x + w)$ would be followed by $\frac{\partial^2}{\partial x^2}\psi(x) \sim \delta(x+w)$. On the contrary the Schrödinger equation (2.16) yields that there is at most a finite jump discontinuity, since $|V_I(x|) < \infty$. That is, indeed, a contradiction to our assumption so that the wavefunction ψ itself and its first derivative $\frac{\partial}{\partial x}\psi$ have to be continuous at $x = \pm w$.
The first condition provides:

$$A_2\left(e^{ik_2w}\pm e^{-ik_2w}\right)=2iA_1e^{ik_1L}\sin\left[k_1(w-L)\right]\;\Leftrightarrow\;A_2=2iA_1e^{ik_1L}\frac{\sin\left[k_1(w-L)\right])}{e^{ik_2w}\pm e^{-ik_2w}}=:A_1\cdot R, \tag{2.28}$$

where we have introduced the abbreviation

$$R=2ie^{ik_1L}\frac{\sin\left[k_1(w-L)\right]}{e^{ik_2w}\pm e^{-ik_2w}}. \tag{2.29}$$

It follows immediately that with this automatically the continuous changeover $\psi_2(w)=\psi_3(w)$ is fullfilled. So we reduce to only one general normalization constant $A_1=:A$ which depends on the parity of the wavefunction via the constant R:

$$R^s=ie^{ik_1^sL}\frac{\sin\left[k_1^s(w-L)\right]}{\cos\left(k_2^sw\right)}\qquad\text{and}\qquad R^a=e^{ik_1^aL}\frac{\sin\left[k_1^a(w-L)\right]}{\sin\left(k_2^aw\right)}. \tag{2.30}$$

2.4 Symmetric states

Now we concentrate on the symmetric solutions of (2.16):

$$\psi_1^s(x)=-2iA^se^{ik_1^sL}\sin\left[k_1^s(x+L)\right], \tag{2.31}$$

$$\psi_2^s(x)=2iA^se^{ik_1^sL}\frac{\sin\left[k_1^s(w-L)\right]}{\cos\left(k_2^sw\right)}\cos(k_2^sx), \tag{2.32}$$

$$\psi_3^s(x)=2iA^se^{ik_1^sL}\sin\left[k_1^s(x-L)\right]. \tag{2.33}$$

In the end of the previous Section we have argued that also the first derivative of the total wavefunction has to be continuous at $x=\pm w$. That provides an additional condition which can be used to determine the complex wavenumbers k_1^s and k_2^s and thus also the complex energies E_1^s and E_2^s via (2.21). We call this the *quantization condition*:

$$\left.\frac{\partial\psi_1^s}{\partial x}\right|_{x=-w}=\left.\frac{\partial\psi_2^s}{\partial x}\right|_{x=-w}\quad\Leftrightarrow\quad-k_1^s\cos\left[k_1^s(w-L)\right]=k_2^s\frac{\sin\left[k_1^s(w-L)\right]}{\cos\left(k_2^sw\right)}\sin(k_2^sw)$$

$$\Leftrightarrow\quad k_1^s\cot\left[k_1^s(w-L)\right]+k_2^s\tan\left(k_2^sw\right)=0. \tag{2.34}$$

Eq. (2.34) is thus the quantization condition for the wavenumbers k_1^s and k_2^s. It is a transcendental equation which can not be solved algebraically. Therefore, we will determine its solutions later numerically.

Finally we can determine A^s by normalizing the full wavefunction (2.17) via

$$\int_{-\infty}^{\infty}\psi^s(x)^*\psi^s(x)\mathrm{d}x=2\int_{-L}^{-w}\psi_1^s(x)^*\psi_1^s(x)\mathrm{d}x+2\int_{-w}^{0}\psi_2^s(x)^*\psi_2^s(x)\mathrm{d}x=1, \tag{2.35}$$

since $\psi^*\psi$ is a symmetric function, because ψ and ψ^* always have the same parity. This yields a real constant

$$|A^s| = \Bigg\{ 2e^{-k^s_{I,1}L} \Bigg[\frac{\sin 2k^s_{R,1}(w-L)}{k^s_{R,1}} - \frac{\sinh 2k^s_{I,1}(w-L)}{k^s_{I,1}} + \frac{\cosh 2k^s_{I,1}(w-L) - \cos 2k^s_{R,1}(w-L)}{\cosh 2k^s_{I,2}w + \cos 2k^s_{R,2}w} \left(\frac{\sinh 2k^s_{I,2}w}{k^s_{I,2}} + \frac{\sin 2k^s_{R,2}w}{k^s_{R,2}} \right) \Bigg] \Bigg\}^{-1/2}, \tag{2.36}$$

where we decomposed $k^s = k^s_R + ik^s_I$ in real and imaginary part, that is $k^s_R, k^s_I \in \mathbb{R}$. We have to state that formally this is only the absolute value of A^s, which is determined up to a phase φ^s that yields an additional factor:

$$A^s = |A^s| e^{i\varphi^s}. \tag{2.37}$$

This phase is quite arbitrary since the physics, i.e. all measurable quantities, are $U(1)$-symmetric so that an additional phase does not change physics. We will choose it later in an appropriate way in the discussion of the real limit to get the familiar real results for the wavefunction of the real potential well.

Now we actually can write the complete symmetric solution of the Schrödinger equation (2.16) for a given imaginary potential V_I. We also solved the time-dependent Schrödinger equation (2.1) so that we can calculate the probability densities and currents for the symmetric states:

$$\rho^s_1(x,t) = 2|A^s|^2 \exp\left[2k^s_{I,1} \left(\frac{\hbar}{M} k^s_{R,1} t - L \right) \right] \left\{ \cosh 2k^s_{I,1}(x+L) - \cos 2k^s_{R,1}(x+L) \right\}, \tag{2.38}$$

$$\rho^s_2(x,t) = 2|A^s|^2 \exp\left[2k^s_{I,1} \left(\frac{\hbar}{M} k^s_{R,1} t - L \right) \right] \tag{2.39}$$

$$\times \frac{\cosh 2k^s_{I,1}(w-L) - \cos 2k^s_{R,1}(w-L)}{\cos 2k^s_{R,2}w + \cosh 2k^s_{I,2}w} \left\{ \cos 2k^s_{R,2}x + \cosh 2k^s_{I,2}x \right\}, \tag{2.40}$$

$$\rho^s_3(x,t) = 2|A^s|^2 \exp\left[2k^s_{I,1} \left(\frac{\hbar}{M} k^s_{R,1} t - L \right) \right] \left\{ \cosh 2k^s_{I,1}(x-L) - \cos 2k^s_{R,1}(x-L) \right\}, \tag{2.41}$$

$$j^s_1(x,t) = \frac{2\hbar}{M} |A^s|^2 \exp\left[2k^s_{I,1} \left(\frac{\hbar}{M} k^s_{R,1} t - L \right) \right] \left\{ k^s_{I,1} \sin 2k^s_{R,1}(x+L) - k^s_{R,1} \sinh 2k^s_{I,1}(x+L) \right\}, \tag{2.42}$$

$$j^s_2(x,t) = \frac{2\hbar}{M} |A^s|^2 \exp\left[2k^s_{I,1} \left(\frac{\hbar}{M} k^s_{R,1} t - L \right) \right] \tag{2.43}$$

$$\times \frac{\cos 2k^s_{R,1}(w-L) - \cosh 2k^s_{I,1}(w-L)}{\cos 2k^s_{R,2}w + \cosh 2k^s_{I,2}w} \left(-k^s_{I,2} \sin 2k^s_{R,2}x - k^s_{R,2} \sinh 2k^s_{I,2}x \right), \tag{2.44}$$

$$j^s_3(x,t) = \frac{2\hbar}{M} |A^s|^2 \exp\left[2k^s_{I,1} \left(\frac{\hbar}{M} k^s_{R,1} t - L \right) \right] \left\{ k^s_{R,1} \sinh 2k^s_{I,1}(x-L) - k^s_{I,1} \sin 2k^s_{R,1}(x-L) \right\}. \tag{2.45}$$

We can confirm that $\rho^s(x,t)$ is a symmetric function while $j^s(x,t,)$ is antisymmetric, since obviously $\rho_1^s(x,t) = \rho_3^s(-x,t)$ and $\rho_2^s(x,t) = \rho_2^s(-x,t)$ as well as $j_1^s(x,t) = -j_3^s(-x,t)$ and $j_2^s(x,t) = -j_2^s(-x,t)$ is fullfilled. The continuity of ρ^s can also directly be seen. One will also be assured by evaluating ρ^s and j^s at $x = \pm w$ that the quantization condition (2.34), which has to be fullfilled by k_1^s and k_2^s, provides differentiability of ρ^s and continuity of j^s right there. The discussion of the continuity equation has already shown that j^s is not differentiable at that points.

We can now compute the continuity equation for the three areas and verify that (2.15) is valid, since according to Eq. (2.21) it is $k_{R,1}^s k_{I,1}^s = \frac{M}{\hbar^2} E_I^s$ and $k_{R,2}^s k_{I,2}^s = \frac{M}{\hbar^2}(E_I^s + C)$ and thus

$$\begin{aligned}\frac{\partial}{\partial t}\rho^s(x,t) + \frac{\partial}{\partial x} j^s(x,t) &= \begin{cases} \frac{2\hbar}{M}\rho_2^s(x,t)\left(k_{R,1}^s k_{I,1}^s - k_{R,2}^s k_{I,2}^s\right) = -\frac{2C}{\hbar}\rho_2^s(x,t), & |x| < w \\ 0, & \text{otherwise} \end{cases} \\ &= \frac{2}{\hbar} V_I(x)\rho^s(x,t). \end{aligned} \tag{2.46}$$

That corresponds, indeed, exactly to the general continuity equation (2.15).

2.4.1 Real limit

Next we check these results for consistency by evaluating them in the limit $C \longrightarrow 0$, the so called real limit, with the aim to get the familiar solutions for E and ψ of the ordinary real potential well.
For $C = 0$ we can directly deduce from (2.21) that $k_1^s = k_2^s =: k^s$ and so the quantization condition (2.34) becomes:

$$\begin{aligned} k^s \tan(k^s w) = -k^s \cot[k^s(w-L)] \quad &\Leftrightarrow \quad \frac{\sin(k^s w)}{\cos(k^s w)} + \frac{\cos[k^s(w-L)]}{\sin[k^s(w-L)]} = 0 \\ &\Leftrightarrow \quad \cos(k^s w)\cos[k^s(w-L)] + \sin(k^s w)\sin[k^s(w-L)] = 0 \\ &\Leftrightarrow \quad \cos(k^s L) = 0. \end{aligned} \tag{2.47}$$

If we decompose this into real and imaginary part

$$\cos k^s L = \cos(k_R^s L)\cosh(k_R^s L) - i\sin(k_R^s L)\sinh(k_R^s L) = 0, \tag{2.48}$$

we can extract two independent conditions for k_R^s and k_I^s. Since $\cosh x$ does not have any real root as well as $\cos x$ and $\sin x$ do not have any mutual root, these conditions have the quite short form:

$$\cos k_R^s L = 0 \qquad \text{and} \qquad \sinh k_I^s L = 0. \tag{2.49}$$

Here $\sinh x$ only vanishes if and only if $x = 0$. Since $L \neq 0$ in general we can conclude that $k_I^s = 0$ and therefore k^s is a real number. Using this we can conclude directly from (2.21) that also the energy E^s becomes real, that is $E_I^s = 0$. The condition $\cos k_R^s L = 0$ yields

$$k_R^s = k_n^s = \frac{\pi}{2L}(2n+1) \qquad \Rightarrow \qquad E^s = E_n^s = \frac{\hbar^2}{2M}(k_n^s)^2 = \frac{\hbar^2\pi^2}{8ML^2}(2n+1)^2, \tag{2.50}$$

which are the energies of the symmetric states of the real potential well for integer n. Next we evaluate the normalization constant for vanishing perturbation. Therefore, we look at Eq. (2.36) and set $k_{I,1}^s = k_{I,2}^s = 0$ and $k_{R,1}^s = k_{R,2}^s = \frac{\pi}{2L}(2n+1) = k^s$. With the help of De L'Hospital we get

$$\lim_{x\to 0} \frac{\sinh ax}{x} = a \tag{2.51}$$

as well as $\cos 2k^s(w-L) = -\cos 2k^s w$ and $\sin 2k^s(w-L) = -\sin 2k^s w$, so we can directly derive the result

$$|A_0^s| = \left\{ 2\left[-\frac{\sin 2k^s w}{k^s} - 2(w-L) + 2w + \frac{\sin 2k^s w}{k^s} \right] \right\}^{-1/2} = \frac{1}{2\sqrt{L}}. \tag{2.52}$$

Finally we check the wavefunction in the unperturbed case. Therefore, we formally distinguish between $\psi_{1,0}^s$ and $\psi_{2,0}^s$ and we will see that the width w drops out so that we end up with $\psi_{1,0}^s = \psi_{2,0}^s$. Formally we have to insert $A^s = \frac{1}{2\sqrt{L}} e^{i\varphi^s}$ instead of (2.52) since we only determined the absolute value of the normalization constant so that an arbitrary phase φ^s additionally occurs. Before inserting all that into the wavefunctions we first give the results of some direct calculations from the value of the unperturbed wave number k^s which will make the following computations clearer:

$$e^{\pm ik_n^s L} = \pm i\xi_n\,, \quad \sin k_n^s(x \pm L) = \pm\xi_n \cos k_n^s x\,, \quad \cos k_n^s(x \pm L) = \mp\xi_n \sin k_n^s x, \tag{2.53}$$

where we have introduced

$$\xi_n := \begin{cases} -1 & , \ n \text{ is odd} \\ +1 & , \ n \text{ is even} \end{cases}. \tag{2.54}$$

If we insert k^s into the symmetric wavefunction in area 1 from (2.31) and 2 from (2.33) and make use of these identities, it is quite straight forward to derive the desired result, where we note that $\xi_n^2 = 1$ for every n:

$$\psi_{1,0}^s(x) = -2i\frac{1}{2\sqrt{L}} e^{i\varphi^s} \cdot i\xi_n \cdot \xi_n \cos k_n^s x = e^{i\varphi^s}\frac{1}{\sqrt{L}} \cos k_n^s x\ , \tag{2.55}$$

$$\psi_{2,0}^s(x) = 2i\frac{1}{2\sqrt{L}} e^{i\varphi^s} \cdot i\xi_n \frac{-\xi_n \cos k_n^s w}{\cos k_n^s w} \cos k_n^s x = e^{i\varphi^s}\frac{1}{\sqrt{L}} \cos k_n^s x, \tag{2.56}$$

which is indeed the same. Because of the symmetry of the cosine function, the condition $\psi_1^s(x) = \psi_3^s(-x)$ is automatically fullfilled so that the barrier at $x = \pm w$ generally vanishes and thus we can describe the whole wavefunction inside the potential well by one single expression:

$$\psi_0^s(x) = e^{i\varphi^s} \frac{1}{\sqrt{L}} \cos k_n^s x. \tag{2.57}$$

By comparing this with the familiar result

$$\psi_0^s(x) = \frac{1}{\sqrt{L}} \cos k_n^s x, \tag{2.58}$$

we can conclude that an appropriate choice for the phase would be $\varphi^s = 0$. Thus the normalization constant A^s is real, that is

$$A^s = |A^s| . \tag{2.59}$$

Now we check the validity of the continuity equation in the case of a real potential. At first we can state that for all three areas the right-hand side of (2.46) has to vanish and according to Eq. (2.9) also the time derivative of the density is equal to zero since $E_I^s = 0$. We can conclude this also from the fact that H is hermitian in the real case, therefore U is an unitary operator and thus $\rho^s(x,t)$ is static and reads

$$\rho_0^s(x,t) = \underbrace{U(t,t_0)U^\dagger(t,t_0)}_{=1} \rho_0^s(x,t_0) = \rho_0^s(x,t_0) = 4\,|A_0^s|^2 \cos^2 k^s x = \frac{1}{L} \cos^2 k^s x, \tag{2.60}$$

which can be also derived from (2.38) – (2.41). Therefore, we have to show for consistency that $\frac{\partial}{\partial x} j_0^s(x,t) = 0$. A direct calculation yields from (2.42) – (2.44) that even $j_0^s \equiv 0$, since $k_I^s = 0$ in the unperturbed case.

2.4.2 Limit of vanishing waist

Finally we check what happens if the perturbation vanishes when the width of area 2 goes to zero. This should have the same effect as evaluating the system for $C \to 0$, i.e. the real limit. We can confirm that this, indeed, comes out of the calculation. We only have to check this for Eq. (2.34) knowing that this is the right background for all results we got for the real limit:

$$\lim_{w\to 0} \left\{ k_2^s \underbrace{\tan\left(k_2^s w\right)}_{\to 0} + k_1^s \cot\left[k_1^s (w - L)\right] \right\} = k_1^s \frac{\cos k_1^s L}{\sin k_1^s L} = 0. \tag{2.61}$$

We can see that k_2^s drops out which is plausible. We neglect the uninteresting case $k_1^s = 0$ but state that k_1^s has to fullfill $\cos k_1^s L = 0$ and thus must be real for the same reasons as in the real limit. Therefore, we call $k^s := k_1^s$ the wavenumber for the whole interval $[-L, L]$, which are area 1 and 3 for vanishing w, and obtain the same results as we got for the real limit.

2.5 Antisymmetric states

Now we evaluate the antisymmetric states of the complex potential well. From Section 2.3 we can deduce the following antisymmetric wavefunctions in area 1 – 3:

$$\psi_1^a(x) = -2iA^a e^{ik_1^a L} \sin\left[k_1^a(x+L)\right], \tag{2.62}$$

$$\psi_2^a(x) = -2iA^a \cdot R^a \sin\left(k_2^a x\right) = -2iA^a e^{ik_1^a L} \frac{\sin\left[k_1^a(w-L)\right]}{\sin\left(k_2^a w\right)} \sin(k_2^a x) \ , \tag{2.63}$$

$$\psi_3^a(x) = -2iA^a e^{ik_1^a L} \sin\left[k_1^a(x-L)\right]. \tag{2.64}$$

With these expressions for the antisymmetric wavefunction we can implement the differentiability at $x = -w$ and thus get the quantization condition of the antisymmetric states:

$$\left.\frac{\partial\psi_1^a}{\partial x}\right|_{x=-w} = \left.\frac{\partial\psi_2^a}{\partial x}\right|_{x=-w} \quad \Leftrightarrow \quad -k_1^a \cos\left[k_1^a(w-L)\right] = -k_2^a \frac{\sin\left[k_1^a(w-L)\right]}{\sin\left(k_2^a w\right)} \cos(k_2^a w)$$

$$\Leftrightarrow \quad k_1^a \cot\left[k_1^a(w-L)\right] - k_2^a \cot\left(k_2^a w\right) = 0. \tag{2.65}$$

Just like in the symmetric case we end up with a transcendental equation that determines k_1^a and k_2^a, which can in general not be solved algebraically. Now we calculate the normalization constant A^a of the antisymmetric states just like we did for the symmetric ones and get:

$$|A^a| = \Bigg\{ 2e^{-2k_{I,1}^a L} \Bigg[\frac{\sin 2k_{R,1}^a(w-L)}{k_{R,2}^a} - \frac{\sinh 2k_{I,1}^a(w-L)}{k_{I,2}^a} + \frac{\cos 2k_{R,1}^a(w-L) - \cosh 2k_{I,1}^a(w-L)}{\cos 2k_{R,2}^a w - \cosh 2k_{I,2}^a w} \left(\frac{\sinh 2k_{I,2}^a w}{k_{I,2}^a} - \frac{\sin 2k_{R,2}^a w}{k_{R,2}^a} \right) \Bigg] \Bigg\}^{-1/2}. \tag{2.66}$$

Just as for the symmetric states we formally have to consider an additional phase to get A^a out of $|A^a|$:

$$A^a = |A^a|\, e^{i\varphi^a}. \tag{2.67}$$

An appropriate choice will be provided by the discussion of the real limit.

Now let us compute the probability density $\rho^a(x,t)$ and the probability current $j^a(x,t)$ for the antisymmetric states:

$$\rho_1^a(x,t) = 2|A^a|^2 \exp\left[2k_{I,1}^a\left(\frac{\hbar}{M}k_{R,1}^a t - L\right)\right]\left\{\cosh 2k_{I,1}^a(x+L) - \cos 2k_{I,1}^a(x+L)\right\}, \tag{2.68}$$

$$\rho_2^a(x,t) = 2|A^a|^2 \exp\left[2k_{I,1}^a\left(\frac{\hbar}{M}k_{R,1}^a t - L\right)\right] \tag{2.69}$$

$$\times \frac{\cos 2k_{R,1}^a(w-L) - \cosh 2k_{I,1}^a(w-L)}{\cos 2k_{R,2}^a w - \cosh 2k_{I,2}^a w}\left\{\cosh 2k_{I,2}^a x - \cos 2k_{R,2}^a x\right\}, \tag{2.70}$$

$$\rho_3^a(x,t) = 2|A^a|^2 \exp\left[2k_{I,1}^a\left(\frac{\hbar}{M}k_{R,1}^a t - L\right)\right]\left\{\cosh 2k_{I,1}^a(x-L) - \cos 2k_{I,1}^a(x-L)\right\}, \tag{2.71}$$

$$j_1^a(x,t) = \frac{2\hbar}{M}|A^a|^2 \exp\left[2k_{I,1}^a\left(\frac{\hbar}{M}k_{R,1}^a t - L\right)\right]\left\{k_{I,1}^a \sin 2k_{R,1}^a(x+L) - k_{R,1}^a \sinh 2k_{I,1}^a(x+L)\right\}, \tag{2.72}$$

$$j_2^a(x,t) = \frac{2\hbar}{M}|A^a|^2 \exp\left[2k_{I,1}^a\left(\frac{\hbar}{M}k_{R,1}^a t - L\right)\right] \tag{2.73}$$

$$\times \frac{\cos 2k_{R,1}^a(w-L) - \cosh 2k_{I,1}^a(w-L)}{\cos 2k_{R,2}^a w - \cosh 2k_{I,2}^a w}\left(k_{I,2}^a \sin 2k_{R,2}^a x - k_{R,2}^a \sinh 2k_{I,2}^a x\right), \tag{2.74}$$

$$j_3^a(x,t) = \frac{2\hbar}{M}|A^a|^2 \exp\left[2k_{I,1}^a\left(\frac{\hbar}{M}k_{R,1}^a t - L\right)\right]\left\{k_{I,1}^a \sin 2k_{R,1}^a(x-L) - k_{R,1}^a \sinh 2k_{I,1}^a(x-L)\right\}. \tag{2.75}$$

We can state the same results concerning symmetry of ρ^a and antisymmetry of j^a as for the symmetric states. A small calculation would show that the quantization condition (2.34), which k_1^a and k_2^a have to fullfill, ensures that ρ^a is differentiable and j^a is continuous at $x = \pm w$. We already found out that j^a could not be differentiable right there.
We can now evaluate the continuity equation for the antisymmetric states and verify that (2.15) is valid also for them, since according to Eq. (2.21) it is $k_{R,1}^a k_{I,1}^a = \frac{M}{\hbar^2}E_I^a$ and $k_{R,2}^a k_{I,2}^a = \frac{M}{\hbar^2}(E_I^a + C)$ and thus

$$\frac{\partial}{\partial t}\rho^a(x,t) + \frac{\partial}{\partial x}j^a(x,t) = \begin{cases} \frac{2\hbar}{M}\rho_2^a(x,t)\left(k_{R,1}^a k_{I,1}^a - k_{R,2}^a k_{I,2}^a\right) = -\frac{2C}{\hbar}\rho_2^a(x,t), & |x| < w \\ 0, & \text{otherwise} \end{cases}$$

$$= \frac{2}{\hbar}V_I(x)\rho_2^a(x,t). \tag{2.76}$$

That corresponds indeed exactly to the general continuity equation (2.15). Therefore, the continuity equation holds for states with both parities.

2.5.1 Real limit

Now we evaluate the antisymmetric states for $C \to 0$ and proceed just like we did for the symmetric states. First we deduce from (2.21) that $k_1^a = k_2^a = k^a$ so that we can solve (2.65) analytically:

$$k^a \cot k^a(w-L) - k^a \cot k^a w = 0 \quad \Leftrightarrow \quad 0 = \cos[k^a(w-L)]\sin(k^a w) - \cos(k^a w)\sin[k^a(w-L)]$$

$$\Leftrightarrow \quad 0 = \sin k^a L. \tag{2.77}$$

Decomposing k^a into real and imaginary part provides

$$\sin k^a L = \cosh(k_I^a L)\sin(k_R^a L) + i\sinh(k_I^a L)\cos(k_R^a L) = 0, \tag{2.78}$$

from which we extract the following two equations

$$\sin(k_R^a L) = 0 \qquad \text{and} \qquad \sinh(k_I^a L) = 0, \tag{2.79}$$

since $\cosh x$ has no real root as well as $\sin x$ and $\cos x$ have no mutual root. This provides that k^a is real just like in the symmetric case and has to fullfill

$$k^a = k_n^a = \frac{n\pi}{L} \qquad \Rightarrow \qquad E^a = E_n^a = \frac{\hbar^2\pi^2}{2ML^2}n^2, \tag{2.80}$$

which are exactly the results from the real potential well for integer n. The normalization constant A^a becomes

$$|A^a| = \left\{2\left[\frac{\sin 2k^a w}{k^a} - 2(w-L) + 2w - \frac{\sin 2k^a w}{k^a}\right]\right\}^{-1/2} = \frac{1}{2\sqrt{L}}, \tag{2.81}$$

since (2.51) as well as $\sin 2k_R^a(w-L) = \sin 2k_R^a w$ and $\cos 2k_R^a(w-L) = \cos 2k_R^a w$ for $k_R^a = \frac{n\pi}{L}$ and $k_I^a = 0$. Now we ensure that the wavefunction, which is separated into 3 parts, turns into the familiar form

$$\psi_n^a(x) = \frac{1}{\sqrt{L}}\sin k_n^a x. \tag{2.82}$$

Therefore, we use some identities which directly follow from $k_n^a = \frac{n\pi}{L}$:

$$e^{\pm ik_n^a L} = \xi_n\,, \quad \sin k_n^a(x \pm L) = \xi_n \sin k_n^a x\,, \quad \cos k_n^a(x \pm L) = \xi_n \cos k_n^a x, \tag{2.83}$$

with ξ_n defined in (2.54). So the antisymmetric wavefunction in area 1 and 2 reads:

$$\psi_1^a(x) = -2ie^{i\varphi^a}\frac{1}{2\sqrt{L}}\xi_n \cdot \xi_n \sin k_n^a x = -ie^{i\varphi^a}\frac{1}{\sqrt{L}}\sin k_n^a x\ \ , \tag{2.84}$$

$$\psi_2^a(x) = -2ie^{i\varphi^a}\frac{1}{2\sqrt{L}}\xi_n\frac{\xi_n \sin k_n^a w}{\sin k_n^a w}\sin k_n^a x = -ie^{i\varphi^a}\frac{1}{\sqrt{L}}\sin k_n^a x, \tag{2.85}$$

since $\xi_n^2 = 1$. The wavefunction in area 3 is determined by $\psi_1^a(x)$ and due to the antisymmetry of the sine function we can deduce that $\psi_1^a = \psi_2^a = \psi_3^a$ in the real case which we denote with ψ_0^a. In the end we clarify the phase φ^a by comparing our result with the solutions (2.82) of the real potential well. Thus we have to choose φ^a so that $-ie^{i\varphi^a} = 1$, that is $\varphi^a = \pi/2$. Therefore, the normalization constant is completely imaginary:

$$A^a = i\,|A^a|\,. \tag{2.86}$$

Finally we evaluate the continuity equation in the real limit, which is quite the same discussion as for the symmetric states. For the same reason the time evolution operator U is unitary for a vanishing imaginary potential. Therefore, the density looses its time dependence:

$$\rho_0^a(x,t) = \underbrace{U(t,t_0)U^\dagger(t,t_0)}_{=1}\rho_0^a(x,t_0) = \rho_0^a(x,t_0) = 4\,|A_0^s|^2 \sin^2 k^a x = \frac{1}{L}\sin^2 k^a x, \tag{2.87}$$

so that its derivative with respect to t is equal to zero. A direct calculation shows from (2.72) – (2.75) that $j_0^a \equiv 0$ so that the continuity equation in the real limit is fullfilled since both terms vanish.

2.5.2 Limit of vanishing waist

We can derive this result also by evaluating $w \to 0$ along the same line as for the symmetric states. We only have to make a slight transformation of Eq. (2.65), that is equivalent to

$$k_2^a \tan k_1^a(w-L) - k_1^a \tan k_2^a w = 0. \tag{2.88}$$

Thus, we can immediately evaluate this expression for $w \to 0$:

$$\lim_{w\to 0}\left\{k_2^a \tan\left[k_1^a(w-L)\right] - k_1^a \underbrace{\tan\left(k_2^a w\right)}_{\to 0}\right\} = k_2^a \frac{\sin k_1^a L}{\cos k_1^a L} = 0. \tag{2.89}$$

One sees that k_2^a drops out again since $k_2^a \neq 0$ and so the new condition is now $\sin k_1^a L = 0$. This is indeed the same condition as for the real limit so that we can call $k_1^a = k^a$ and adopt completely its results to the limit of vanishing waist.

3 Numerical analysis

Both quantization conditions (2.34) and (2.65) are transcendental equations and are, therefore, not solvable in an algebraic way. Thus, we have to find its solutions $k_1 = k_1(C)$ and $k_2 = k_2(C)$ numerically. Both variables depend on the energy $E = E(C)$ so that we can rewrite (2.34) and (2.65) in terms of the energy to have an equation only depending on one variable, which is more comfortable to solve.

3.1 Some further theoretical discussion

Before starting with the numerical calculation it is useful to have some further theoretical insights of the so far derived formulas. This will make it easier to have an appropriate physical interpretation of the numerical results afterwards.

3.1.1 Dimensionless variables

First of all we express all variables in a dimensionless way. Therefore, we use from now on the following dimensionless quantities:

$$\varepsilon := \frac{E}{\frac{\hbar^2}{2M}\left(\frac{\pi}{2L}\right)^2}, \qquad c := \frac{C}{\frac{\hbar^2}{2M}\left(\frac{\pi}{2L}\right)^2}, \qquad \kappa := \frac{k}{\frac{\pi}{2L}}, \qquad \chi := \frac{x}{\frac{2L}{\pi}}, \qquad \omega := \frac{w}{\frac{2L}{\pi}}. \tag{3.1}$$

In terms of these new variables the quantization conditions (2.34) and (2.65) now read

$$0 = \kappa_1^s \cot\left[\kappa_1^s\left(\omega - \frac{\pi}{2}\right)\right] + \kappa_2^s \tan\left(\kappa_2^s \omega\right) \quad , \tag{3.2}$$

$$0 = \kappa_1^a \cot\left[\kappa_1^a\left(\omega - \frac{\pi}{2}\right)\right] - \kappa_2^a \cot\left(\kappa_2^a \omega\right). \tag{3.3}$$

If we reexpress (2.21) in terms of the new variables

$$\kappa_1 = \sqrt{\varepsilon} \qquad \text{and} \qquad \kappa_2 = \sqrt{\varepsilon + ic}, \tag{3.4}$$

we can rewrite (3.2) and (3.3) for a given dimensionless waist ω as a function of only one complex quantity $\varepsilon = \varepsilon(c)$:

$$0 = \sqrt{\varepsilon^s} \cot\left[\left(\omega - \frac{\pi}{2}\right)\sqrt{\varepsilon^s}\right] + \sqrt{\varepsilon^s + ic} \tan\left(\omega\sqrt{\varepsilon^s + ic}\right) \quad , \tag{3.5}$$

$$0 = \sqrt{\varepsilon^a} \cot\left[\left(\omega - \frac{\pi}{2}\right)\sqrt{\varepsilon^a}\right] - \sqrt{\varepsilon^a + ic} \cot\left(\omega\sqrt{\varepsilon^a + ic}\right). \tag{3.6}$$

The symmetric wavefunctions (2.31) – (2.33) now read:

$$\psi_1^s(\chi) = -2iAe^{i\kappa_1^s \frac{\pi}{2}} \sin\kappa_1^s \left(\chi + \frac{\pi}{2}\right) \ , \tag{3.7}$$

$$\psi_2^s(\chi) = 2iAe^{i\kappa_1^s \frac{\pi}{2}} \frac{\sin\kappa_1^s \left(\omega - \frac{\pi}{2}\right)}{\cos\kappa_2^s \omega} \cos\kappa_2^s \chi \ , \tag{3.8}$$

$$\psi_3^s(\chi) = \psi_1^s(-\chi) = 2iAe^{i\kappa_1^s \frac{\pi}{2}} \sin\kappa_1^s \left(\chi - \frac{\pi}{2}\right) \ , \tag{3.9}$$

whereas the antisymmetric ones (2.62) – (2.64) reduce to

$$\psi_1^a(\chi) = -2iAe^{i\kappa_1^a \frac{\pi}{2}} \sin\kappa_1^a \left(\chi + \frac{\pi}{2}\right) \ , \tag{3.10}$$

$$\psi_2^a(\chi) = -2iAe^{i\kappa_1^a \frac{\pi}{2}} \frac{\sin\kappa_1^a \left(\omega - \frac{\pi}{2}\right)}{\sin\kappa_2^a \omega} \sin\kappa_2^a \chi \ , \tag{3.11}$$

$$\psi_3^a(\chi) = -\psi_1^a(-\chi) = -2iAe^{i\kappa_1^a \frac{\pi}{2}} \sin\kappa_1^a \left(\chi - \frac{\pi}{2}\right). \tag{3.12}$$

Since the normalization constant A has still the dimension $1/\sqrt{L}$, the densities $\rho(\chi) = \psi(\chi)^* \psi(\chi)$ scale with $1/L$ as it should be.

3.1.2 Limit of big waist

It will turn out to be quite useful to have some initial theoretical discussion of (3.5) and (3.6) before solving them for several ω and c. We have already done the "limit of vanishing waist", that is $\omega \to 0$, and got the familiar case of the real potential well, that is $\varepsilon_I = 0$. We can consider this as a kind of simple limit case for the potential well getting real again. However, we did not yet evaluate the other extreme case $w \to L$, that is $\omega \to \frac{\pi}{2}$. Therefore, we consider Eqs. (3.2) and (3.3) again and calculate this limit. We start with (3.2) and have to change it a bit:

$$0 = \lim_{\omega \to \pi/2} \left\{ \kappa_1^s \underbrace{\cos\left[\kappa_1^s \left(\omega - \frac{\pi}{2}\right)\right]}_{\to 1} \cos(\kappa_2^s \omega) + \underbrace{\kappa_2^s \sin(\kappa_2^s \omega) \sin\left[\kappa_1^s \left(\omega - \frac{\pi}{2}\right)\right]}_{\to 0} \right\}$$

$$0 = \cos\left(\kappa_2^s \frac{\pi}{2}\right), \tag{3.13}$$

since $\kappa_1^s \neq 0$. With the same argumentation as in the real limit this could only be fullfilled if and only if κ_2^s is a real number, more precisely an odd integer one, that is $\kappa_2^s = 2n+1$ where n is an integer number. With (3.4) this means

$$\kappa_2^s = \sqrt{\varepsilon_R^s + i(\varepsilon_I^s + c)} \ \stackrel{!}{=} 2n+1 \in \mathbb{Z} \quad \Rightarrow \quad \varepsilon_I^s = -c, \ \ \varepsilon_R^s = (2n+1)^2. \tag{3.14}$$

For the antisymmetric states we get the same result. If we change (3.3) a bit we get:

$$0 = \lim_{\omega\to\pi/2}\left\{\kappa_1^a \underbrace{\cos\left[\kappa_1^a\left(\omega-\frac{\pi}{2}\right)\right]}_{\to 1}\sin\left(\kappa_2^a\omega\right) - \kappa_2^a\cos\left(\kappa_2^a\omega\right)\underbrace{\sin\left[\kappa_1^a\left(\omega-\frac{\pi}{2}\right)\right]}_{\to 0}\right\}$$

$$0 = \sin\left(\kappa_2^a\frac{\pi}{2}\right). \tag{3.15}$$

This is also a result which is fullfilled by $\kappa_2^a = 2n$ for integer n as we found out in Subsection 2.5.1. Therefore, we can conclude from (3.4):

$$\kappa_2^a = \sqrt{\varepsilon_R^a + i(\varepsilon_I^a + c)} \stackrel{!}{=} 2n \in \mathbb{Z} \quad \Rightarrow \quad \varepsilon_I^a = -c,\ \ \varepsilon_R^a = (2n)^2, \tag{3.16}$$

which is indeed the same result for ε_I.

Thus we can state that these two kinds of limits for the waist ω yield two different conditions for the imaginary part of the energy ε_I, that is

$$\lim_{\omega\to 0}\varepsilon_I = 0 \qquad \text{and} \qquad \lim_{\omega\to\pi/2}\varepsilon_I = -c. \tag{3.17}$$

It is an interesting fact that both limits of ω actually represent the real limit since we receive the same wavenumbers for the nonvanishing area. Therefore, we will get the same wavefunctions as in the real case. We will see in the evaluation of the numerical solutions that there is a quite plausible reason for this observation.

3.2 Energies

3.2.1 Solutions

It is quite straight forward to find the roots of the left-hand side of (3.5) and (3.6) numerically for given c and ω. In our dimensionless variables the energy of the symmetric states for vanishing perturbation reads $\varepsilon_{R,n}(0) = (2n+1)^2$ thus the symmetric ground state for the real potential well is characterized by $n = 0$ in (2.50). For the antisymmetric states this condition reads $\varepsilon_{R,n}(0) = (2n)^2$ and thus it seems to be comfortable to assign to every energy of a symmetric state the natural number $m := 2n+1$ and to every antisymmetric state $m := 2n$. Therefore, all states denoted with an odd m are symmetric while all states denoted with an even m are antisymmetric. Thus the symmetric ground state is denoted by ε_1, the first antisymmetric excited state by ε_2 and so on. We can conclude that every reasonable solution of (3.5) *and* (3.6) has now to fullfill $\varepsilon_{R,m}(0) = m^2$ and $\varepsilon_{I,m}(0) = 0$ like we found out in the discussion of the real limit. This new assignment will make it easier to do a general evaluation of all states in the potential well.
For increasing values of the dimensionsless waist ω we find the corresponding results shown in Figs. 3 and 4:

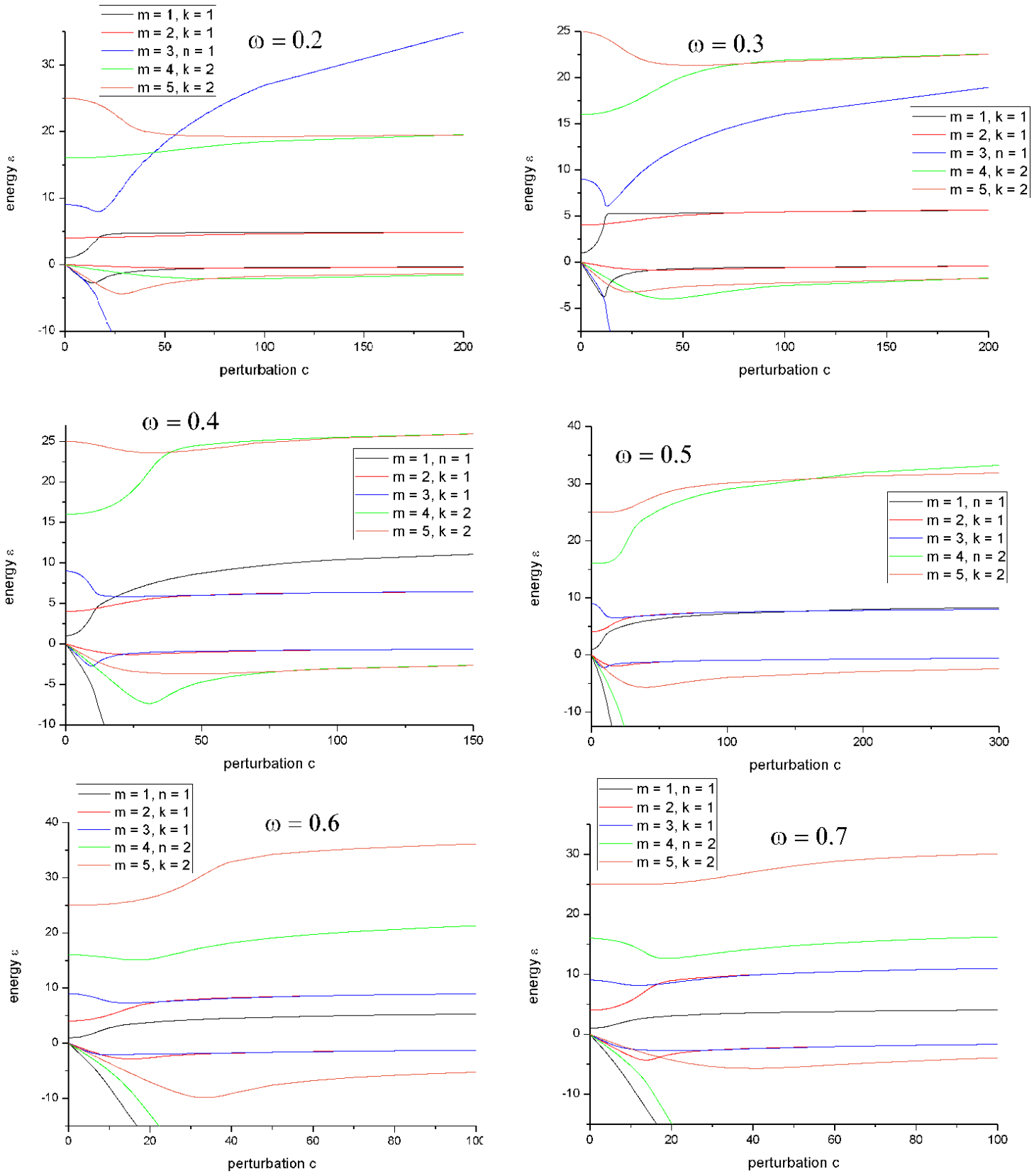

Figure 3: Real and imaginary part of the lowest energy eigenvalues as a function of the strength c of the imaginary potential for the waists $\omega = 0.2 - 0.7$. Two curves with the same colour represent the real and imaginary part of the energy of the state, whereat the real part starts at $\varepsilon_R(c = 0) = m^2$ and the imaginary part at $\varepsilon_I(c = 0) = 0$. Moreover, ε_∞-states are counted by integer n while ε_0-states are counted by integer k.

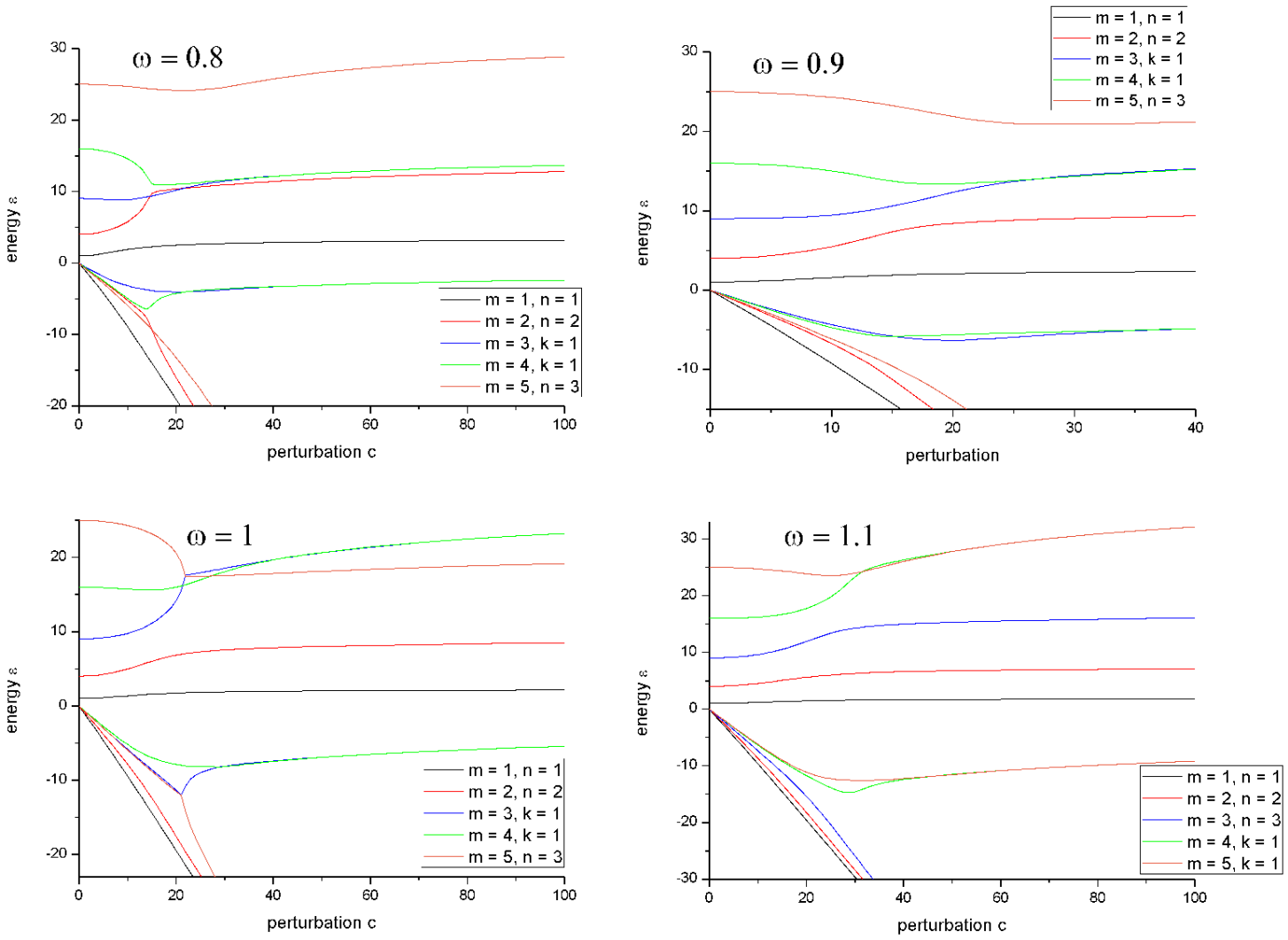

Figure 4: Real and imaginary part of the lowest energy eigenvalues as a function of the strength c of the imaginary potential for the waists $\omega = 0.8 - 1.1$. Two curves with the same colour represent the real and imaginary part of the energy of the state, whereat the real part starts at $\varepsilon_R(c = 0) = m^2$ and the imaginary part at $\varepsilon_I(c = 0) = 0$. Moreover, ε_∞-states are counted by integer n while ε_0-states are counted by integer k.

It is interesting to see that one can generally divide all states into two groups. The states of the one group, which we denote by ε_∞, has a divergent imaginary part which goes for a large imaginary potential linearly to infinity, while the states of the other group have an imaginary part which goes to zero for large c so that we denote them with ε_0. Furthermore, every ε_0–state approaches to another ε_0–state with the other parity so that we can observe pairs of one antisymmetric and one symmetric ε_0–state for $c \to \infty$ which tend to the same limit $\lim_{c\to\infty} \varepsilon_0$.
For increasing imaginary potential of strength c the states behave more and more like in the case of $\omega \to 0$ and $\omega \to \pi/2$. Moreover, one can state that for small ω there are more ε_0–states among the lowest 5 energy levels, while the number of ε_∞–states increases for higher ω in that group of states with lower energy. It seems that the assignment of a state to the group of ε_∞– or ε_0–states strongly depends on the saturation value of the real part of its energy ε_R, while it apparently does not depend on parity or the energy value the state is starting at for $c = 0$. There

seems to be no obvious rule for this classification but a look at the numerical solutions for large values c gives the impression that it has to do something with the order of the saturation values of the first 5 states. If we neglect the behaviour for small c the real part of the energy of every plotted state is monotonously increasing for large c and arrives at some finite saturation value as we can conclude from the numerical solutions. These values seem to depend on the waist ω in a way that the saturation values of ε_R of ε_∞–states are decreasing with ω while these of the ε_0–state are increasing with ω. Therefore, for increasing waists the lower energy levels become ε_∞ while the ε_0–states are pushed to higher energy levels. In Figs. 3 and 4 we can observe that the states starting at low energies of the real potential well, that is $c = 0$, for example the energies of the states $m = 1$ or $m = 2$ of the real potential well, are ε_0 for small waists like $\omega = 0.2$ and become ε_∞ for large waists like $\omega = 1.1$. Thus we can see that the essential order of the energies is not seriously changed so that there has to be a kind of replacement of ε_0 states by ε_∞–states for some critical values of ω. For $\omega = 0.3$, 0.8, 1 one can observe an unusual development of the two involved states which for lower c attract and from some c on reject each other. For increasing c they are getting closer and closer at this specific c and then something remarkable happens. At some critical waist ω_{crit} the "upper" state, which is a ε_∞ one, is not rejected any more by the lower ε_0–state but changes roles with it. An intersection occurs and the state starting at the lower energy, i.e. $c = 0$, now becomes the new ε_∞ one and has the larger saturation value while the former ε_∞, which started at the higher level, now is ε_0 and fuses with the opposite parity state in between converging to the lower saturation value of the real part of the energy. We can observe this phenomenon in more detail by evaluating, for instance, the progress of the $m = 1$– and $m = 3$–state in the range, where ω increases from 0.3 to 0.33 as shown in Fig. 5:

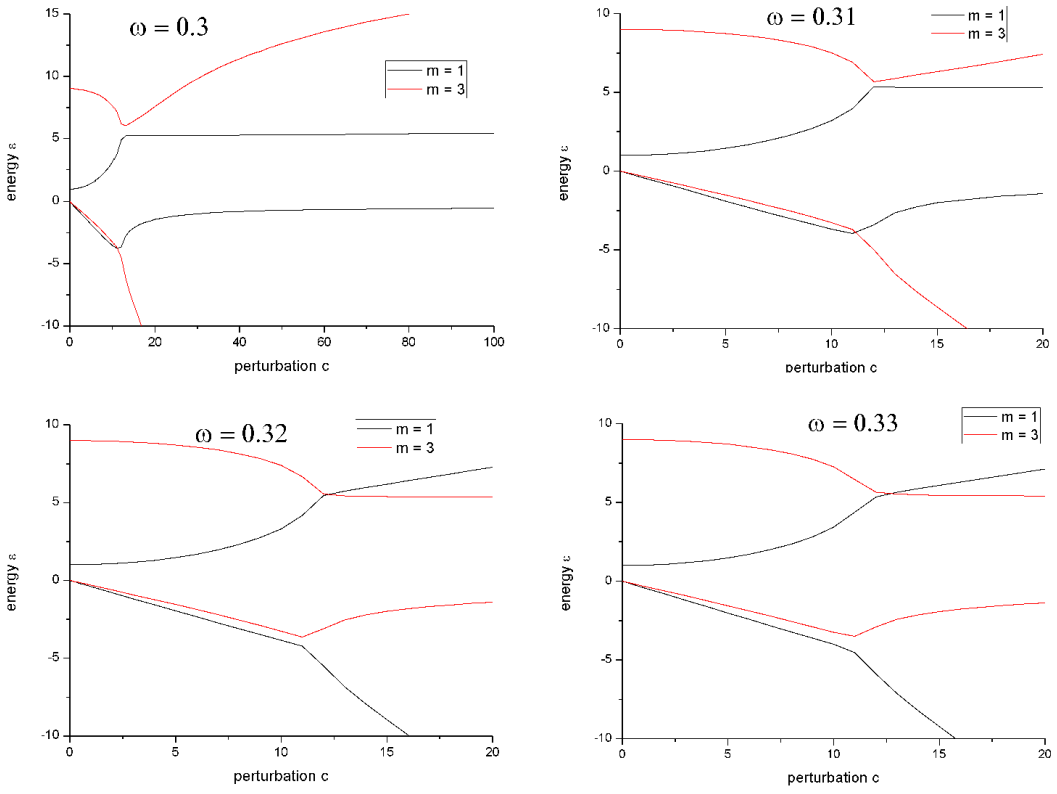

Figure 5: Change of ε_0- and ε_∞–states near the critical waist.

It is not possible to determine the exact ω_{crit} graphically because it depends on the assignment of particular solutions of (3.5) to the one or the other curve which seems to be quite arbitrary since both possible curves do not change in a sufficiently traceable way. We have already found out that the saturation value of the real part of ε_0–states increases with c, while for ε_∞–states it decreases with c. Moreover, we know that also the particular assignment whether a state is ε_0 or ε_∞ has something to do with its saturation value. The question of the exact ω_{crit} and the occurrence of the intersection is thus an additional motivation to revisit the quantization conditions and to calculate the saturation value of ε_R for $c \to \infty$. This should be ω-dependent and contain some kind of *quantum number* to enumerate the different ε_0– and ε_∞–states, which we already called k and n. This shall provide at least a condition for the intersection of two states which does not change roles for larger waists ω. This property is important since otherwise one will not see any indication for an intersection in the ε–ω–diagram because the ε_∞–state stays the upper one before and after ω_{crit}. In other words the ε-ω-diagram does not know any m which contains the information where a state starts for $c = 0$. Another interesting issue that may be then explained is the fusion of two states with different parities that tend to the same energy limit.
At this point it seems to be reasonable to spend some time on calculating the repeatedly mentioned saturation value of the real part of the energies.

3.2.2 Saturation value for real part of energy

Now we evaluate the saturation value of the real part of the energy ε_R from the transcendental equations (3.5) and (3.6). We start with the symmetric one:

$$\sqrt{\varepsilon^s}\cot\left[\left(\omega-\frac{\pi}{2}\right)\sqrt{\varepsilon^s}\right]+\sqrt{\varepsilon^s+ic}\tan\left[\omega\sqrt{\varepsilon^s+ic}\right]=0. \tag{3.18}$$

By inserting the two empirically known kinds $\varepsilon_{I,\infty}$ and $\varepsilon_{I,0}$ of behaviour of the imaginary part ε_I for $c \to \infty$, that is

$$\lim_{c\to\infty}\varepsilon^s_{I,\infty}=-\lim_{c\to\infty}c \qquad \text{and} \qquad \lim_{c\to\infty}\varepsilon^s_{I,0}=0, \tag{3.19}$$

we are confident to get a corresponding result for the real part ε^s_R. We start with ε_∞. Inserting $\varepsilon^s_{I,\infty} \to -c$ into (3.5) provides

$$\sqrt{\varepsilon^s_{R,\infty}-ic}\cot\left[\left(\omega-\frac{\pi}{2}\right)\sqrt{\varepsilon^s_{R,\infty}-ic}\right]+\sqrt{\varepsilon^s_{R,\infty}}\tan\left[\omega\sqrt{\varepsilon^s_{R,\infty}}\right]=0. \tag{3.20}$$

Since $\varepsilon_R \in \mathbb{R}$ in any case the second term on the left-hand side is already real. Therefore, we split up the first one. To do this we use the polar expression of complex numbers $z = x + iy$

$$z=|z|e^{i\phi}=\sqrt{x^2+y^2}e^{i\arctan\frac{y}{x}}, \tag{3.21}$$

where $x, y \in \mathbb{R}$. For the square root of complex numbers then follows directly:

$$\sqrt{z}=\sqrt{|z|}e^{\frac{i}{2}\phi}=\left(x^2+y^2\right)^{1/4}e^{\frac{i}{2}\arctan\frac{y}{x}}. \tag{3.22}$$

We use this for the expression $\sqrt{\varepsilon^s_{R,\infty} - ic}$ in Eq. (3.20):

$$\sqrt{\varepsilon^s_{R,\infty} - ic} = \left[\left(\varepsilon^s_{R,\infty}\right)^2 + c^2\right]^{1/4} \exp\left[-\frac{i}{2}\arctan\frac{c}{\varepsilon^s_{R,\infty}}\right]. \tag{3.23}$$

Since $\varepsilon^s_{R,\infty}$ tends to some finite value, we can approximate the absolute value by $\left[\left(\varepsilon_{R,\infty}\right)^2 + c^2\right]^{1/4} \approx \sqrt{c}$ and get for the phase

$$\lim_{c\to\infty} \arctan\frac{c}{\varepsilon^s_{R,\infty}} = (2j+1)\frac{\pi}{2}\ , \quad j \in \mathbb{Z}. \tag{3.24}$$

This yields the phase $-\frac{\pi}{4}(2j+1)$, which leads to four formally distinct solutions:

$$\sqrt{c}\exp\left[-i\frac{\pi}{4}(2j+1)\right] = \sqrt{\frac{c}{2}}\begin{cases} 1-i & ,\ j = 0,4,8,... \\ -(1+i) & ,\ j = 1,5,9,... \\ -(1-i) & ,\ j = 2,6,10,... \\ 1+i & ,\ j = 3,7,11,... \end{cases}. \tag{3.25}$$

If we insert this into the first term of the left-hand side of (3.20), we can directly conclude that, since cotangens is an odd function, always two solutions, which only differ from each other by a global minus sign, are equivalent in this case. Therefore, we only have to distinguish between the cases $\sqrt{\frac{c}{2}}(1+i)$ and $\sqrt{\frac{c}{2}}(1-i)$, that is between even and odd numbers j.
We start with odd j. Inserting $\sqrt{\varepsilon^s_{R,\infty} + ic} \approx \sqrt{\frac{c}{2}}(1+i)$ into the first term on the left-hand side of (3.20) provides

$$\sqrt{\frac{c}{2}}(1+i)\cot\left[\sqrt{\frac{c}{2}}(1+i)\left(\omega - \frac{\pi}{2}\right)\right] = \sqrt{\frac{c}{2}}(1+i)\frac{-\sin\left[\sqrt{2c}\left(\omega-\frac{\pi}{2}\right)\right] + i\sinh\left[\sqrt{2c}\left(\omega-\frac{\pi}{2}\right)\right]}{\cos\left[\sqrt{2c}\left(\omega-\frac{\pi}{2}\right)\right] - \cosh\left[\sqrt{2c}\left(\omega-\frac{\pi}{2}\right)\right]}. \tag{3.26}$$

Since $\cos x \in [-1,1]$ for all $x \in \mathbb{R}$ and $\lim_{x\to\infty}\cosh x = \infty$ we can neglect the cosine in the denominator of (3.26). For the same reason we can replace $(1+i)(-\sin x + \sinh x)$ by $-(1-i)\sinh x$ for $x \to \infty$. These approximations provide

$$\sqrt{\frac{c}{2}}(1-i)\underbrace{\frac{\sinh\left[\sqrt{2c}\left(\omega-\frac{\pi}{2}\right)\right]}{\cosh\left[\sqrt{2c}\left(\omega-\frac{\pi}{2}\right)\right]}}_{\to 1} \approx \sqrt{\frac{c}{2}}(1-i). \tag{3.27}$$

Therefore, we can approximate the first term on the left-hand side of (3.20) by the complex expression $\sqrt{\frac{c}{2}}(1-i)$. The same calculation for even j yields a positive imaginary part, that is $\sqrt{\frac{c}{2}}(1+i)$. The resulting equation reads

$$\sqrt{\frac{c}{2}}(1\pm i) + \sqrt{\varepsilon^s_{R,\infty}}\tan\left[\omega\sqrt{\varepsilon^s_{R,\infty}}\right] = 0. \tag{3.28}$$

For the saturation value of $\varepsilon^s_{R,\infty}$ we have to evaluate the real part of this equation which is the same in both cases of j:

$$\sqrt{\frac{c}{2}} + \sqrt{\varepsilon^s_{R,\infty}} \tan\left[\omega\sqrt{\varepsilon^s_{R,\infty}}\right] = 0. \tag{3.29}$$

The first term tends obviously to infinity which can only be compensated if the tangens has a singularity at the saturation value. This means:

$$\omega\sqrt{\varepsilon^s_{R,\infty}} = (2n-1)\frac{\pi}{2} \quad \Leftrightarrow \quad \varepsilon^{s,n}_{R,\infty} = (2n-1)^2\frac{\pi^2}{4\omega^2} \ , \quad n \in \mathbb{Z}. \tag{3.30}$$

For ε^s_0 we get instead of (3.20):

$$\sqrt{\varepsilon^s_{R,0}} \cot\left[\left(\omega - \frac{\pi}{2}\right)\sqrt{\varepsilon^s_{R,0}}\right] + \sqrt{\varepsilon^s_{R,0} + ic} \tan\left[\omega\sqrt{\varepsilon^s_{R,0} + ic}\right] = 0. \tag{3.31}$$

We can see that in this case the first term of the left-hand side is already real so let us find the complex decomposition of the second term. We will do so with the same approach via polar expression as we did for ε^s_∞. Then we finally end up with

$$\sqrt{\frac{c}{2}}(-1 \pm i) + \sqrt{\varepsilon^s_{R,0}} \cot\left[\sqrt{\varepsilon^s_{R,0}}\left(\omega - \frac{\pi}{2}\right)\right] = 0. \tag{3.32}$$

One can see that only the real part contains ε_R. Therefore, we only evaluate this part of the equation since the imaginary part does not provide anything reasonable so that the used approximation seems not to be appropriate for it. The real part of this equation yields that cotangens has to have a singularity at $\sqrt{\varepsilon^s_{R,0}}\left(\omega - \frac{\pi}{2}\right)$. We can thus conclude:

$$\sqrt{\varepsilon^s_{R,0}}\left(\omega - \frac{\pi}{2}\right) = k\pi \quad \Leftrightarrow \quad \varepsilon^{s,k}_{R,0} = \frac{k^2\pi^2}{\left(\omega - \frac{\pi}{2}\right)^2} \ , \quad k \in \mathbb{Z}. \tag{3.33}$$

The same calculations for the antisymmetric states and their quantization condition

$$\sqrt{\varepsilon^a} \cot\left[\sqrt{\varepsilon^a}\left(\omega - \frac{\pi}{2}\right)\right] - \sqrt{\varepsilon^a + ic} \cot\left(\omega\sqrt{\varepsilon^a + ic}\right) = 0 \tag{3.34}$$

yields the following saturation values for ε^a_R:

$$\varepsilon^{a,n}_{R,\infty} = \frac{n^2\pi^2}{\omega^2} \quad \text{and} \quad \varepsilon^{a,k}_{R,0} = \frac{k^2\pi^2}{\left(\omega - \frac{\pi}{2}\right)^2}. \tag{3.35}$$

Note that we used for consistency k and n and defined them in a way that both are starting at 1. Furthermore, we notice the remarkable result that $\varepsilon^{s,k}_{R,0} = \varepsilon^{a,k}_{R,0}$ for each value of k which can be proved by inspecting the respective graphs. This corresponds to the observation that always two

ε_0–states with different parities are becoming one state for $c \to \infty$.
It may clarify to ignore the particular parity of the saturation values, since it obviously does not matter for the ε_0–states. Thus we can write for convenience

$$\varepsilon^n_{R,\infty} = \frac{n^2\pi^2}{4\omega^2} \qquad \text{and} \qquad \varepsilon^k_{R,0} = \frac{k^2\pi^2}{\left(\omega - \frac{\pi}{2}\right)^2} \tag{3.36}$$

and note for $\varepsilon^n_{R,\infty}$ that even n are standing for antisymmetric states and odd n for symmetric ones.

3.2.3 Discussion

We can read off from (3.36) an interesting connection to the energies of a real potential well which confirms our suggestion from Subsection 3.1.2 that for $c \to \infty$ an effective potential well within $\pm\omega$ occurs. If we take the original variables instead of the dimensionless ones this will be obvious. From (3.36) we read off at first

$$E^n_{R,\infty} = \frac{\hbar^2}{2M}\frac{\pi^2}{4L^2}\frac{n^2\pi^2}{4}\frac{4L^2}{\pi^2 w^2} = \frac{\hbar^2\pi^2}{8Mw^2}n^2. \tag{3.37}$$

Comparing this result with the energies of the real potential well (2.50) and (2.80), we conclude that we received the energy of a potential well with the width $2w$ where we note that symmetric and antisymmetric states are included in this formula. Similarly we get for the other formula

$$E^n_{R,0} = \frac{\hbar^2}{2M}\frac{\pi^2}{4L^2}\frac{n^2\pi^2}{4}\frac{4L^2}{\pi^2(w-L)^2} = \frac{\hbar^2\pi^2}{8M(L-w)^2}n^2, \tag{3.38}$$

which are the energies of a potential well with the width $L - w$ that is the outer region of the waist. This insight and the good accordance to the numerical solutions ensures us that we found serious and plausible formulas to calculate the real part of the energy in the limit $c \to \infty$.

By taking a look at the results graphically in Fig. 6, one can see that the convention to mix up symmetric and antisymmetric states is quite reasonable, since the parity of the corresponding state does not matter and we count all energies of one type by only one integer number.

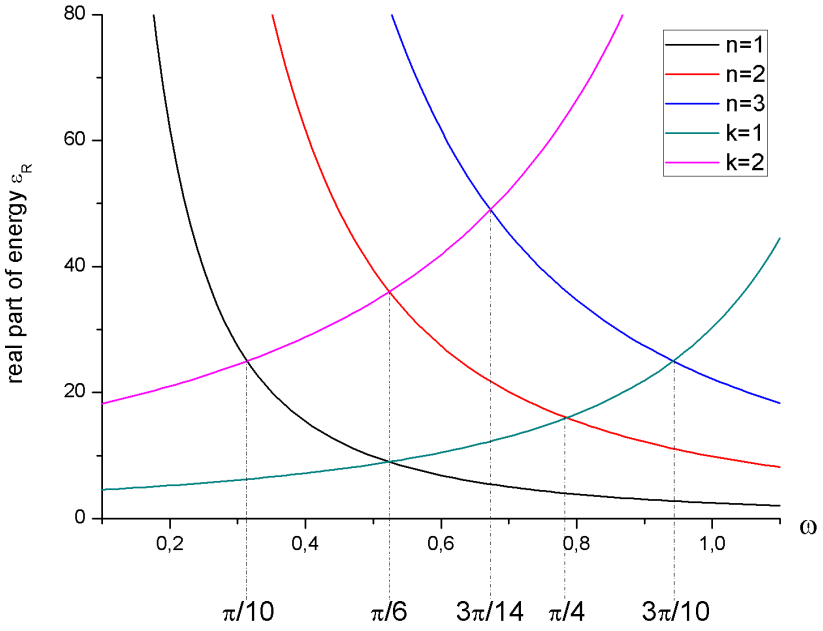

Figure 6: Saturation values of the real part of the energy $\varepsilon_R(\omega)$ for ε_0–states counted by k and ε_∞–states counted by n.

The intersections in Fig. 6 confirm the occuring intersections of the particular states in Figs. 3 and 4. Like we suspected it is only possible to calculate the intersection of two states if they keep their character. This is always fullfilled if the involved ε_∞–state is first the upper one so that after the corresponding critical value the saturation value of the corresponding ε_0–state is higher. This process can be directly seen from the derived formulas (3.36) since ε_0 is strictly monotonic decreasing while ε_∞ is strictly monotonic increasing in the considered interval $\omega \in [0, \pi/2]$. As we already argued these formulas unfortunately do not provide any new information about the occurring process running vice verca with a change of the behaviour of both involved states after it. However it catches the eye that each one of these processes occurs for nearly the same ω where a process of the other kind appears. Since we have already argued that there can not be any strict rule to determine ω_{crit} we have to make an agreement for which ω the change precisely occurs. Let us thus connect this value to the corresponding intersection in Fig. 6 so that the 3 values of ω_{crit} we can read off from Figs. 3 and 4 are $\pi/10$, $\pi/4$ and $\pi/3$. The intersection at $\omega = \pi/3$ does not occur in Fig. 6 because the corresponding states are for example $\varepsilon^1_{R,\infty}$ and $\varepsilon^4_{R,0}$ which are not plotted together in this graph.

Finally, let us discuss boundaries of the considered interval of ω. We know that $\varepsilon_I = 0$ for $\omega \to 0$. Therefore, we only evaluate ε_0 for this boundary since obviously $\lim_{\omega\to 0} \varepsilon_{R,\infty} = \infty$. As we have already seen in the Subsections 2.4.2 and 2.5.2 this should provide the real limit, that is $\varepsilon_R = k^2$. Unfortunately (3.36) yields

$$\lim_{\omega\to 0} \varepsilon^k_{R,0} = 4k^2 \ . \tag{3.39}$$

This looks inconsistent but actually it is not since the approximation we used does not hold for

$\omega = 0$ because the area, where the imaginary potential acts at, vanishes. Therefore, the resulting formula does not have any reference to the problem since the approximation is based on $c \gg \varepsilon_R$ which does not make any sense if c is not involved in the problem any more.
This argumentation is supported by the fact that the evaluation of the other boundary $\omega \to \pi/2$ provides the correct result. As we know from Subsection 2.5.2 the considered energies are ε_∞ as we can also see from the corresponding formula that yields $\lim_{\omega\to\pi/2} \varepsilon_{R,0} = \infty$. Taking the limit of the other one leads to:

$$\lim_{\omega\to\pi/2} \varepsilon^n_{R,\infty} = n^2. \tag{3.40}$$

These are the dimensionless energies of the real potential well which should occur for $\omega \to \pi/2$ as we found out in Subsection 3.1.2.

All in all we can state that in the case of a pure potential well, whereat it does not matter whether it is real or imaginary as we have seen in Subsection 3.1.2, there occurs only one kind of energies that we called ε_0 and ε_∞. In the case of $0 < \omega < \pi/2$, that is two nested potential wells, these kinds of states are mixed. That means that both types are occurring simultaneously. However one can observe and calculate from (3.36) that for small waists there are more ε_0–states appearing for low energies since ε_∞ is really high for small waists while for $\omega \to \pi/2$ the ε_0–states are vanishing from our focus because their energy goes to infinity and the ε_∞–states take their place as the energies of the emerging potential well. This trend is quite obvious from the development of the energy states with ω one can observe from Figs. 3 and 4.

3.3 Densities

3.3.1 Solutions

With (3.5) and (3.6) we can directly calculate from $\varepsilon(c)$ numerical solutions for the dimensionless wavenumbers $\kappa_1(c)$ and $\kappa_2(c)$ via (3.4) and (3.22):

$$\kappa_1 = \left[\varepsilon_R^2 + \varepsilon_I^2\right]^{1/4} \cos\left(\frac{1}{2}\arctan\frac{\varepsilon_I}{\varepsilon_R}\right) + i\left[\varepsilon_R^2 + \varepsilon_I^2\right]^{1/4} \sin\left(\frac{1}{2}\arctan\frac{\varepsilon_I}{\varepsilon_R}\right), \tag{3.41}$$

$$\kappa_2 = \left[\varepsilon_R^2 + (\varepsilon_I + c)^2\right]^{1/4} \cos\left(\frac{1}{2}\arctan\frac{\varepsilon_I + c}{\varepsilon_R}\right) + i\left[\varepsilon_R^2 + (\varepsilon_I + c)^2\right]^{1/4} \sin\left(\frac{1}{2}\arctan\frac{\varepsilon_I + c}{\varepsilon_R}\right). \tag{3.42}$$

Thus it is possible to evaluate the corresponding wavefunctions $\psi(\chi)$ and densities $\rho(\chi)$ for the diverse behaviour of $\varepsilon(c)$ we have so far studied. Nevertheless it seems to be quite tedious to evaluate *all* densities for every waist, perturbation and energy. Therefore, it will turn out to be sufficient to evaluate only some selected examples to bring out the main statement. That means we plot the densities of some ε_0- and ε_∞–states and discuss them. Note that now it makes sense to distinguish between symmetric and antisymmetric states since it will turn out to be interesting how the parity of the state evolves with c. Therefore, since ε_0–states are counted by k and ε_∞–states by n, the parity of ε^n_∞ is given by n, that is symmetric if n is odd and antisymmetric if n is even. The parity of ε^k_0 is given by k in a similar way. Moreover, we used dimensionless densities, that means to get the correct dimension we have to multiply each result with $2\pi/L$.

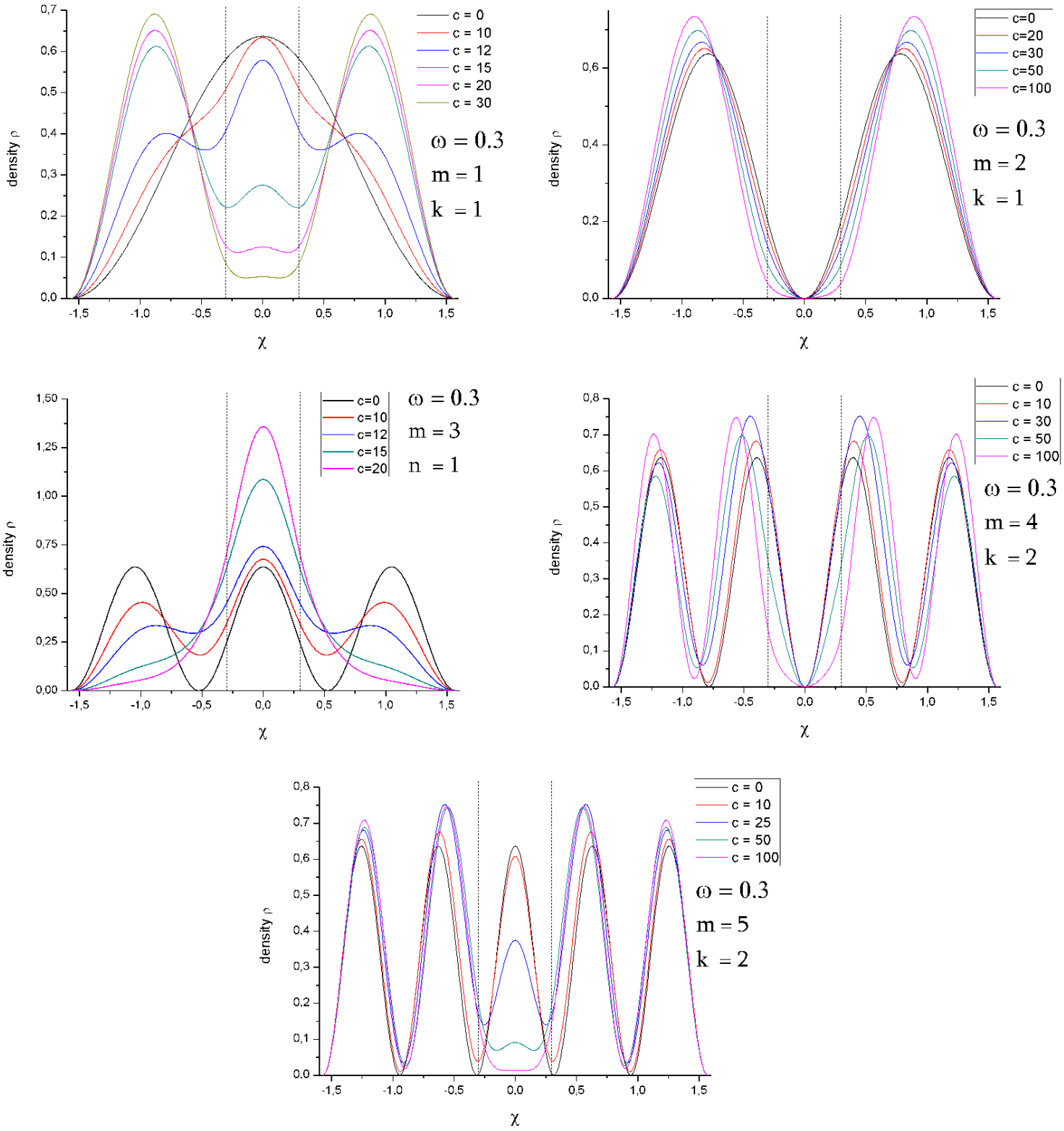

Figure 7: Densities of the lowest energies for $\omega = 0.3$ for some values of c, where all states are counted by m for $c = 0$ and by k if they are ε_0 and by n if they are ε_∞ for $c \to \infty$. The fusion of respectively two ε_0-states, which we already observed in Figs. 3 and 4, is confirmed here. Furthermore, it shows that two states with the same k end up exactly in the same state.

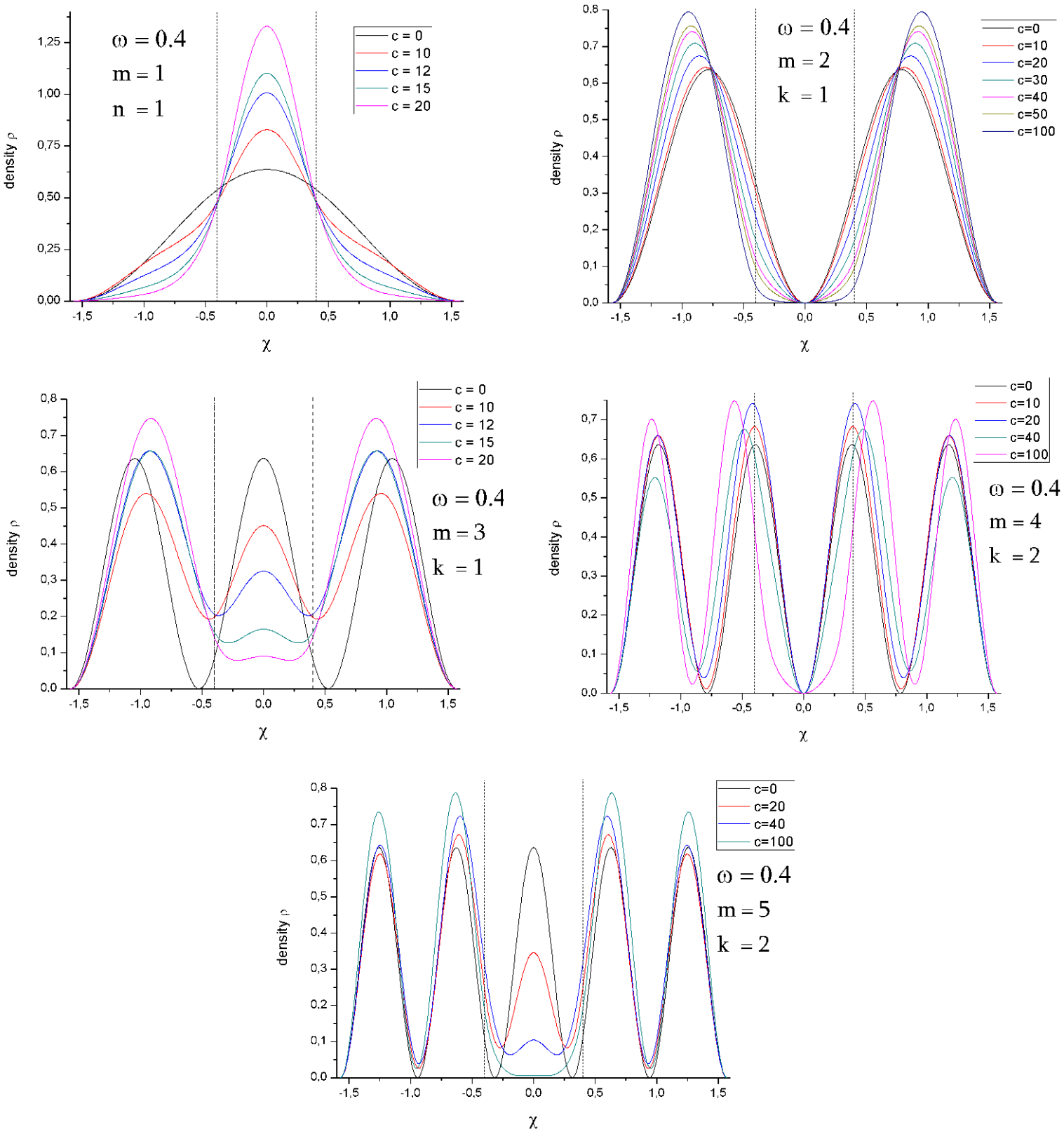

Figure 8: Densities of the lowest energies for $\omega = 0.4$ for some values of c, where all states are counted by m for $c = 0$ and by k if they are ε_0 and by n if they are ε_∞ for $c \to \infty$. The fusion of respectively two ε_0-states, which we already observed in Figs. 3 and 4, is confirmed here. Furthermore, it shows that two states with the same k end up exactly in the same state.

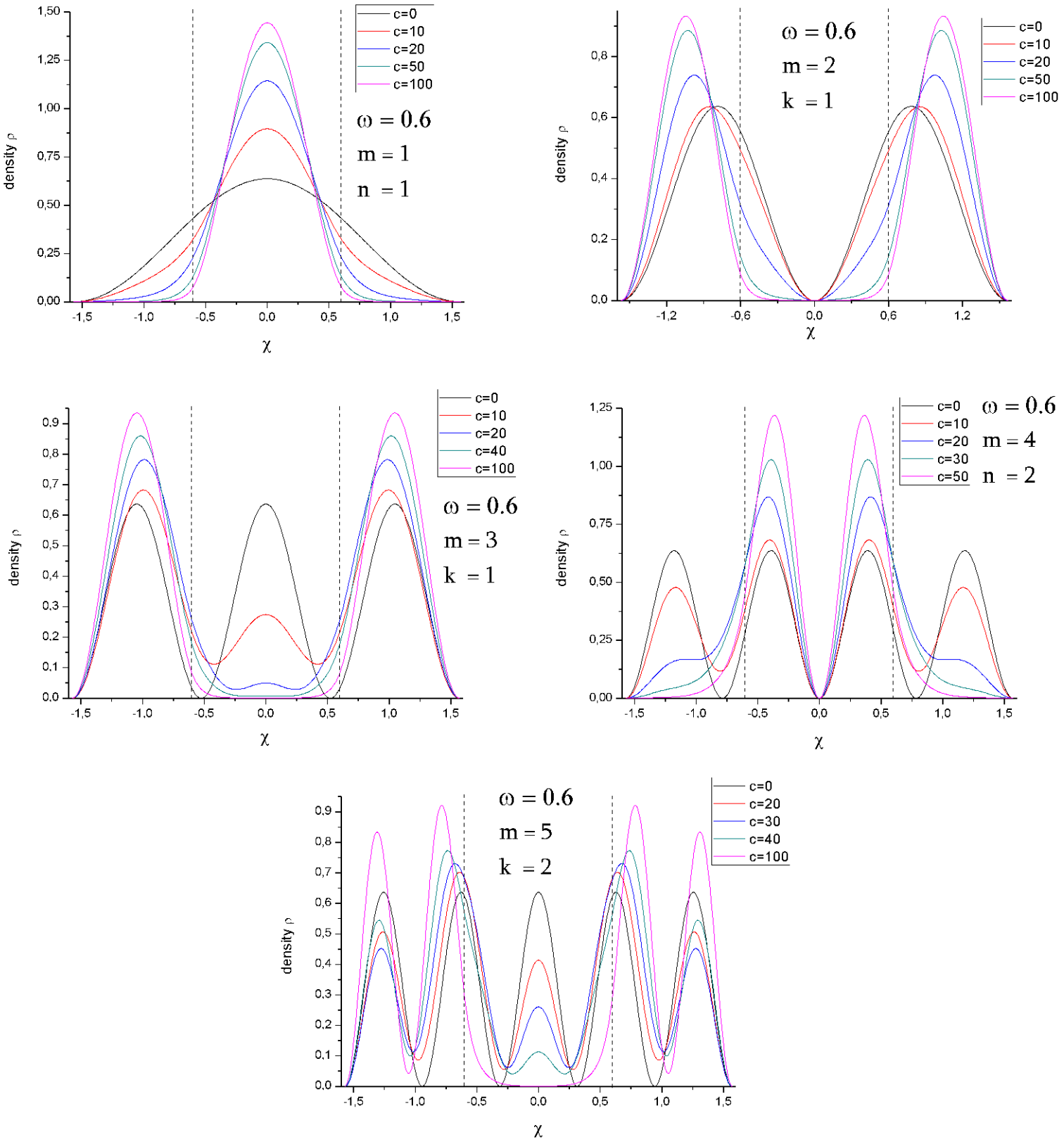

Figure 9: Densities of the lowest energies for $\omega = 0.6$ for some values of c, where all states are counted by m for $c = 0$ and by k if they are ε_0 and by n if they are ε_∞ for $c \to \infty$. The fusion of respectively two ε_0-states, which we already observed in Figs. 3 and 4, is confirmed here. Furthermore, it shows that two states with the same k end up exactly in the same state.

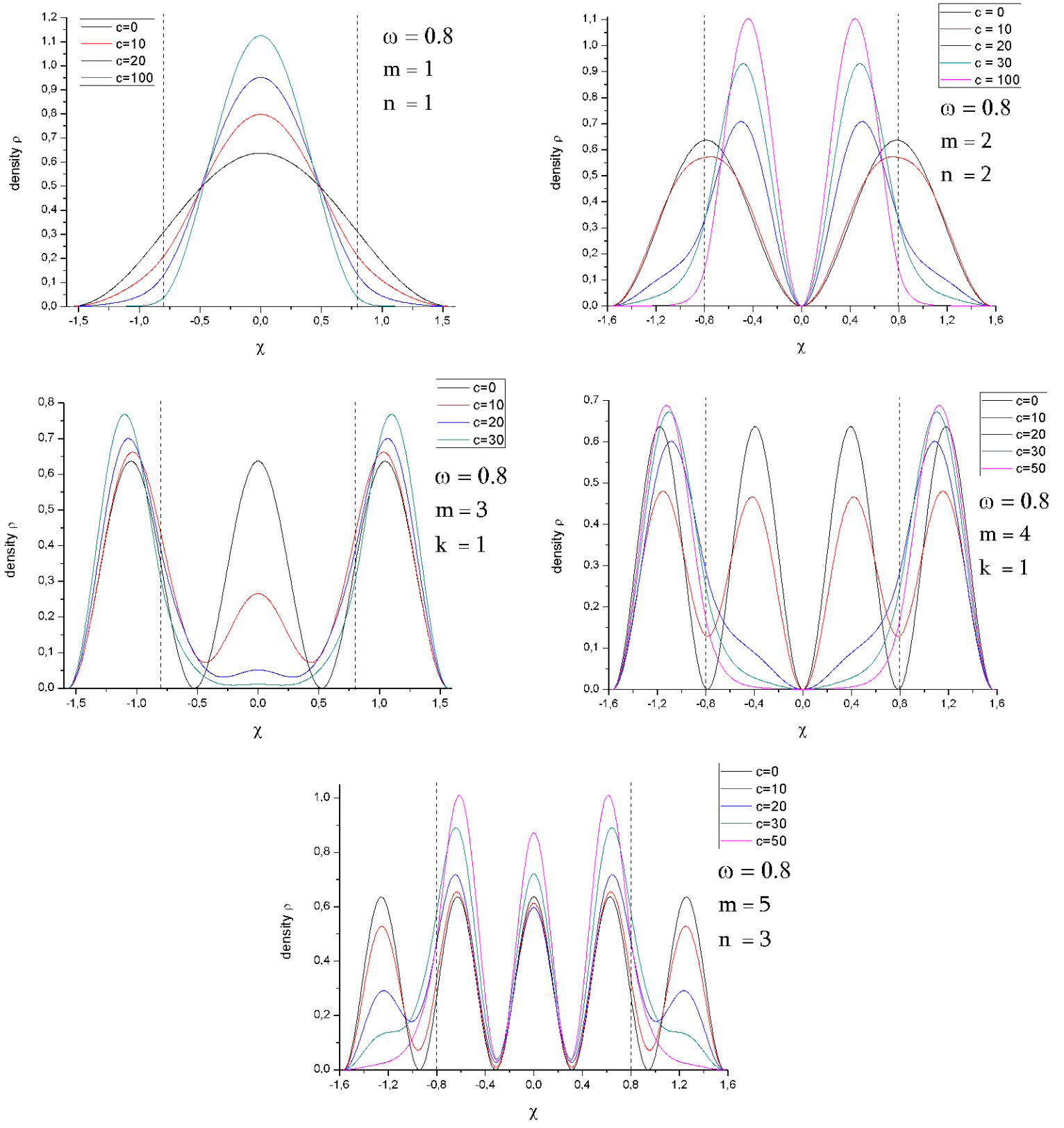

Figure 10: Densities of the lowest energies for $\omega = 0.8$ for some values of c, where all states are counted by m for $c = 0$ and by k if they are ε_0 and by n if they are ε_∞ for $c \to \infty$. The fusion of respectively two ε_0-states, which we already observed in Figs. 3 and 4, is confirmed here. Furthermore, it shows that two states with the same k end up exactly in the same state.

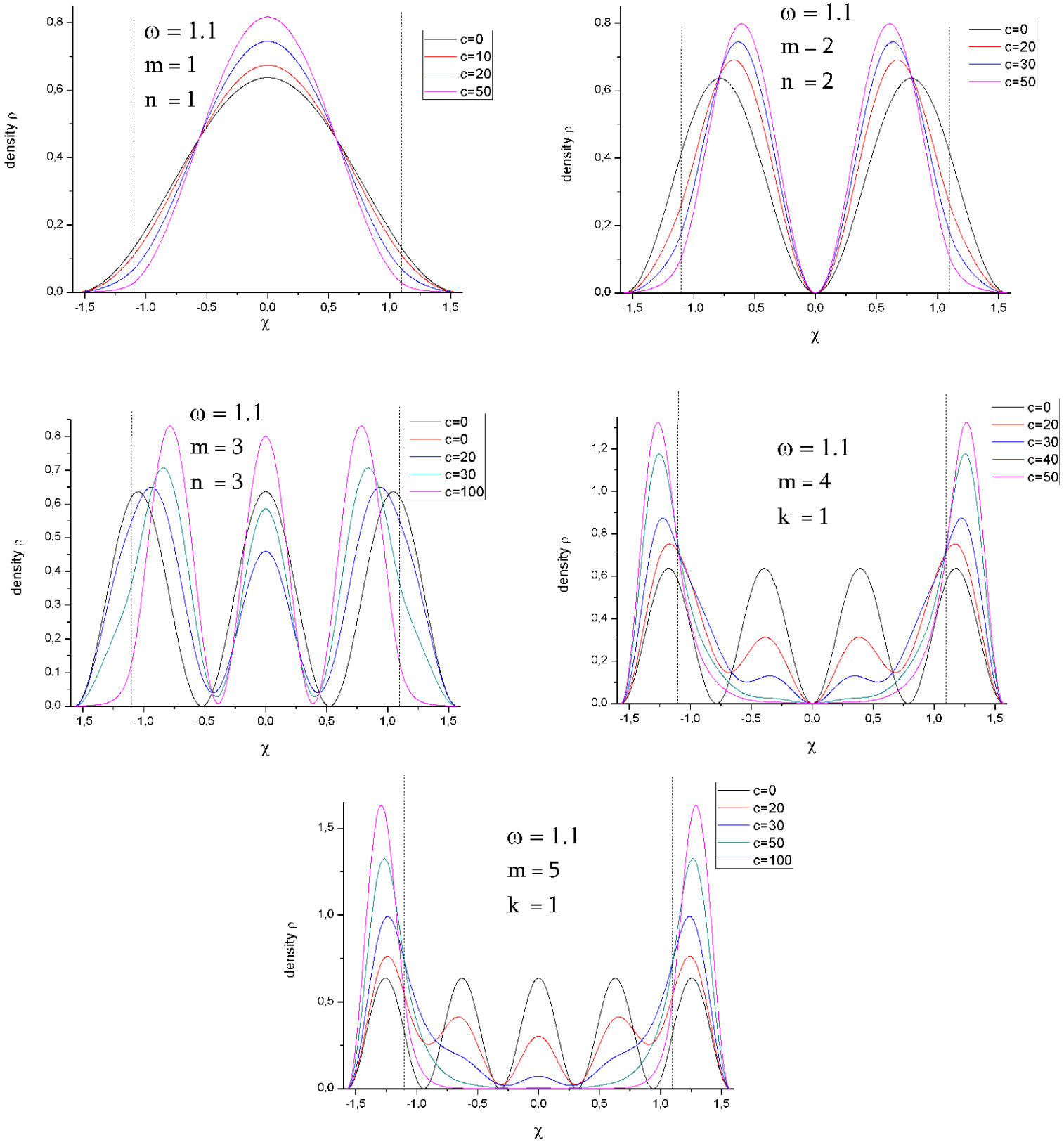

Figure 11: Densities of the lowest energies for $\omega = 1.1$ for some values of c, where all states are counted by m for $c = 0$ and by k if they are ε_0 and by n if they are ε_∞ for $c \to \infty$. The fusion of respectively two ε_0-states, which we already observed in Figs. 3 and 4, is confirmed here. Furthermore, it shows that two states with the same k end up exactly in the same state.

3.3.2 Discussion

Figs. 7 – 11 allow a very deep insight in what is really happening with the energies and states in this nested complex potential well. We already found out that in the case of vanishing waist $\omega \to 0$ the imaginary part of the energy vanishes, too, that is $\varepsilon_I = 0$. Thus we are left with only ε_0–states, which are the familiar states of the real potential well, because the energy of the ε_∞–states tends to infinity. If we take the opposite case of $\omega \to \pi/2$ then only ε_∞–states are remaining, because in this case the energy of ε_0–states diverges. In contrast to ε_0–states they are complex which yields an imaginary part of the energy that corresponds exactly to the strength of the perturbation or rather the depth of the imaginary potential well, that is $\varepsilon_I = -c$. Therefore, we can conclude that the ε_0–states are these of the real potential well as we already found out in the discussion of the real limit, while the ε_∞–states are the states of the imaginary potential well with the depth c, which is also confirmed by (3.37) and (3.38). They are quite the same states and energies, as we found out in the discussion of the energy, with only one difference. There is an imaginary part of the energy which yields the depth of the imaginary well. This could be already concluded from the discussion of the energy.
Now let us have a concreter look at the densities. One can directly observe the distinct behaviour of ε_0–states, which are denoted by the integer number k, and ε_∞–states, which are denoted by the integer number n. A general tendency is that the maxima of probability are shifted in a quite logical way. The maxima of ε_0–states tend to area 1 and 3, while ε_∞–states have maxima in area 2. The probability in the respective outer region, that is area 1 and 3 for ε_∞ and area 2 for ε_0, decreases rapidly for increasing perturbation. A logical consequence of this is that the symmetric ε_0–states are vanishing because a maximum in the center of the well would be a contradiction to this general development. Therefore, the only possible ε_0–states are antisymmetric which have a vanishing probability in the center of the well. For increasing c the maxima are displaced to the borders of the well while in the inner region of the waist the probability decreases. Thus it looks plausible that the symmetric states approach the nearest respective antisymmetric state and are absorbed by it as we found out in the discussion in Section 3.2. This explains the fusion of each pair of one symmetric and one antisymmetric we have already seen in Figs. 3 and 4. The result is one antisymmetric state, whose probability maxima get out of the waist–region, and thus its energy increases with ω.
The ε_∞–states behave vice verca. For $\omega \to 0$ they can not occur because their energy tends to infinity. Because the imaginary potential well is in the center we can observe also symmetric states. The probability in area 1 and 3 decreases for increasing c while the probability maxima are shifted into the waist-region $|\chi| < \omega$. Thus for increasing perturbation a new completely imaginary potential well emerges in the center of the whole potential well with symmetric and antisymmetric states and a rapidly decreasing probability in the outside which is equal to zero for $c \to \infty$. One could also interpret that, for very large c, the potential well is divided twice so that every area is itself a potential well with symmetric and antisymmetric states.
One interesting issue is the shifting of the maxima in the respective region. This could be well seen in Fig. 10 of the $m = 2$–state with $\omega = 0.8$, which is ε_∞, so that the density maxima tend into the center. For $c = 0$ this is an antisymmetric state with two maxima which does not change with perturbation. But we can observe that the maxima become more narrow and in the end are also displaced. The interesting fact is that first they become a bit broader and smaller and for one

specific c the actual development to the final result starts. A closer look at this state in the energy diagram (Fig. 3) shows us that there happens something interesting for $c \in [10, 20]$. Therefore, let us have a closer look at this particular state for these values of perturbation:

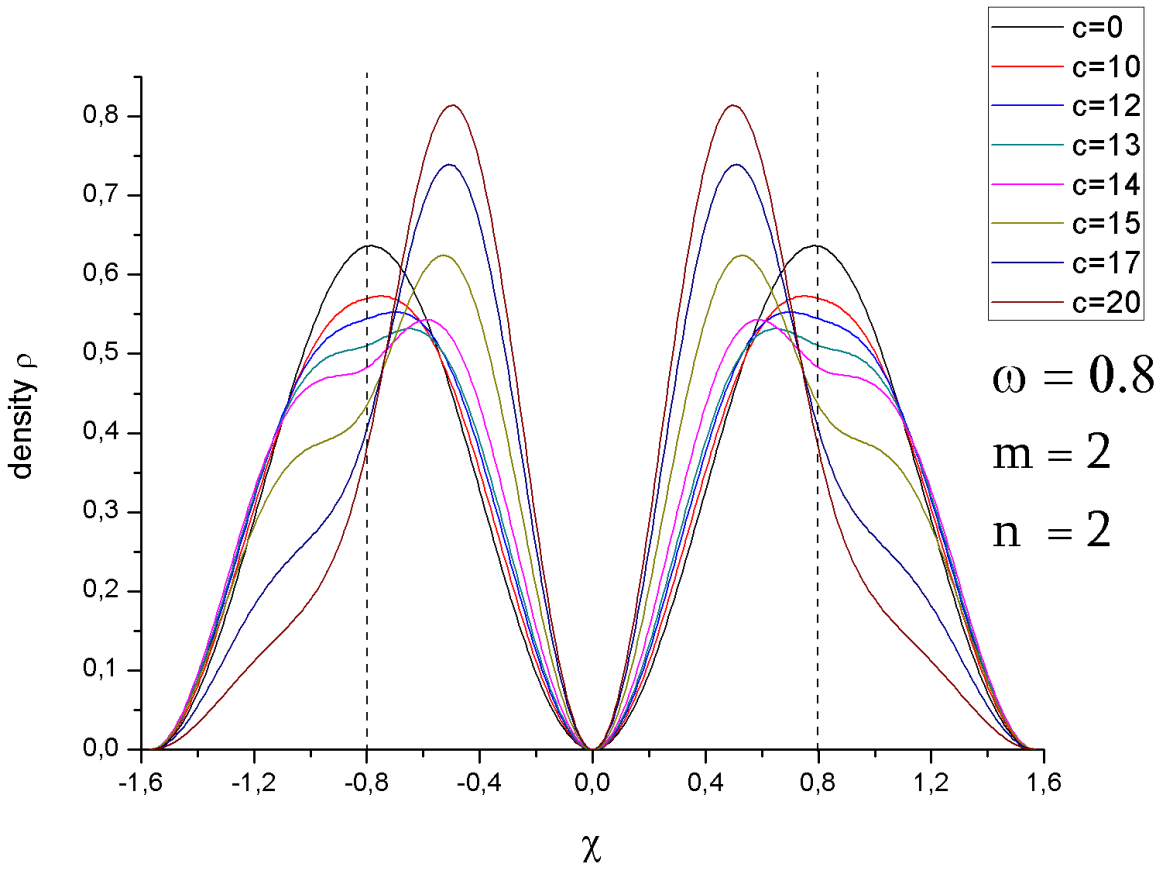

Figure 12: Shifting of the maxima of $m = 2$–state for $\omega = 0.8$ for $c \in [10, 20]$. Both maxima are divided into two parts in the waist region. The parts in area 2 increase and become more narrow peaks while the parts in area 1 and 3 decrease to zero.

In Fig. 12 one can see that the maximum divides into 2 parts since the border between area 1 and 2, that is $|\chi| = \omega$, runs nearly through the middle of the peak. The slightly bigger part is in area 2 so that this part grows while the other one reduces with increasing c so that in the end there remains a narrow peak inside of area 2 and a decay to zero outside.

3.3.3 Critical waists

We have already seen that for $c \to \infty$ the potential well is divided and each area becomes a new real (area 1 and 3) or imaginary (area 2) potential well. So at the end we are left with 3 independent potential wells. The states of the former single real potential well for $c = 0$ are divided up into the 3 new wells where we can genereally distinguish between states shifted to the inside, that is area 2, whose imaginary part of the energy tends to $-\infty$ and states shifted to the outside, that is area 1 and 3, whose imaginary part vanishes for $c \to \infty$. The special assignment

of the states into these two groups depends obviously on the waist and at "critical waists" this assignment is changed. Unfortunately we did not find out a rule for the occurrence of such critical waists. We have rather argued in Subsection 3.2.1 that there is no compulsory rule that tells us when the assignment exactly changes since we only work with single numerical values instead of analyzable functions. In the discussion of Fig. 6 in Subsection 3.2.3 we have found out that the calculated intersections, which unfortunately have nothing to do with the change of the assignment into ε_0 and ε_∞, are though very near to waists where one can observe such a change of assignment. Therefore, the only "rule" we have postulated so far is that each change of assignment emerges precisely at the value of a waist where such an intersection occurs.
In the case of the antisymmetric first excited $m = 2$–state for $\omega = 0.8$, that we have just disussed, it seems to be quite obvious to determine a critical waist from this discussion. This case is insofar special as this state remains a first excited state for $c \to \infty$ namely of the imaginary potential well in area 2. For the argumentation it is important that the state keeps its particular form, that is it remains antisymmetric with two maxima. Let us take a look at Fig. 10 at the states $m = 2$ and $m = 4$. In both cases there is a little bit more area within the waist so that it should take less energy to reduce the outer part of the peak as well as more energy to reduce the inner part and get a narrow peak in the outer region. If we consult the corresponding energy diagram in Fig. 4 we can see that these states are special ones because their energies are very close and we know from our discussion of the energy by comparing with $\omega = 0.7$ that the red and the green curve just have changed roles. That means that for $\omega = 0.7$ the $\varepsilon_\infty^{n=2}$–state has more energy and the $\varepsilon_0^{k=1}$ less while the situation is vice verca for $\omega = 0.8$. We also already know that sequences of energies only depend on the real parts of the energy of the states, that means a replacement occurs, if due to the change of the waist, the energy of an ε_0–state, which increases with ω, becomes higher than the energy of an ε_∞–state, which decreases with ω. It turned out that those replacements are much more interesting than the intersections we calculated in Subsection 3.2.1 since these ones occur between two states of distinct kinds which keep their character and the comparison of a state of the outer and the inner region is, indeed, not very exciting.
We just stated that for example in the case of $\omega = 0.8$ the $m = 2$–state becomes the $\varepsilon_\infty^{n=2}$–state because it is the state of lesser energy than the $\varepsilon_0^{k=1}$–state, that the former $m = 4$–state tends to for $c \to \infty$. This seems to be backed by the following. For the $m = 2$–state we have seen that there is less probability in the outer region than in the inner one so that it seems plausible that the state reduces the probability outside and increase the probability in the inside. This process should need less energy than vice verca like the $m = 4$–state does, which is thus the high-energy one. Therefore, we try to calculate ω_{crit} with this new ansatz that a ε_0–state becomes ε_∞ if for $c = 0$ there is more probability in the inner region than in the outer which only depends on ω as it should.
First we try to calculate the critical waist for this example that is the change of the $m = 2$–state, which is a antisymmetric one, from ε_0 to ε_∞ which is already completed for $\omega = 0.8$. This should occur for the zero-crossing of the following difference

$$0 = \int_{-\pi/2}^{-\omega} |\psi_0^a(\chi)|^2 \, \mathrm{d}\chi - \int_{-\omega}^{0} |\psi_0^a(\chi)|^2 \, \mathrm{d}\chi \tag{3.43}$$

$$= \int_{-\pi/2}^{-\omega} \sin^2 2\chi \mathrm{d}\chi - \int_{-\omega}^{0} \sin^2 2\chi \mathrm{d}\chi, \tag{3.44}$$

since $\kappa_{n=2} = 2$ for $c = 0$. This yields

$$\pi + \sin 4\omega = 4\omega \tag{3.45}$$

which is a transcendental equation but is obviously solved by $\omega = \pi/4$. The same calculation for $m = 4$ also yields the same solution which seems to be plausible. A look at Fig. 5 confirms that this result fits very well and Fig. 6 tells us that there is already an intersection between two states, which does not change, at $\omega = \pi/4$. This confirms the agreement we have made in the discussion of Fig. 6. Unfortunately this method only works if the state keeps its form, that is symmetry and the number of maxima. We can confirm this by applying it on states, which do not fullfill this condition, i.e. the $m = 1$–state for $\omega = 0.8$:

$$0 = \int_{-\pi/2}^{-\omega} \cos^2 \chi \mathrm{d}\chi - \int_{-\omega}^{0} \cos^2 \chi \mathrm{d}\chi \tag{3.46}$$

$$\Leftrightarrow \quad 0 = 4\omega - \pi + 2\sin 2\omega, \tag{3.47}$$

which is solved by $\omega \approx 0.416$. This result does not characterize the situation seriously since we already saw grafically that the respective critical waist has to be about $\omega_{\mathrm{crit}} = \pi/10 \approx 0.314$. The results of the other states also give quite unrealistic results and moreover they do not coincide with 0.416 which leads us to the assumption that this consideration works only for states which keep their form.

3.4 Currents

3.4.1 Solutions

Finally we evaluate the currents (2.42) – (2.45) and (2.72) – (2.75), which we calculated in Sections 2.4 and 2.5. Therefore, we use the same notations and quantities introduced in Section 3.3 and also observe the currents only for the 5 waists we used for the densities. That means states counted by k are ε_0 and such counted by n are ε_∞.

Note that we only plot dimensionless currents. Thus every result has to be multiplied with a factor $\hbar/M$ to get the correct physical dimension.

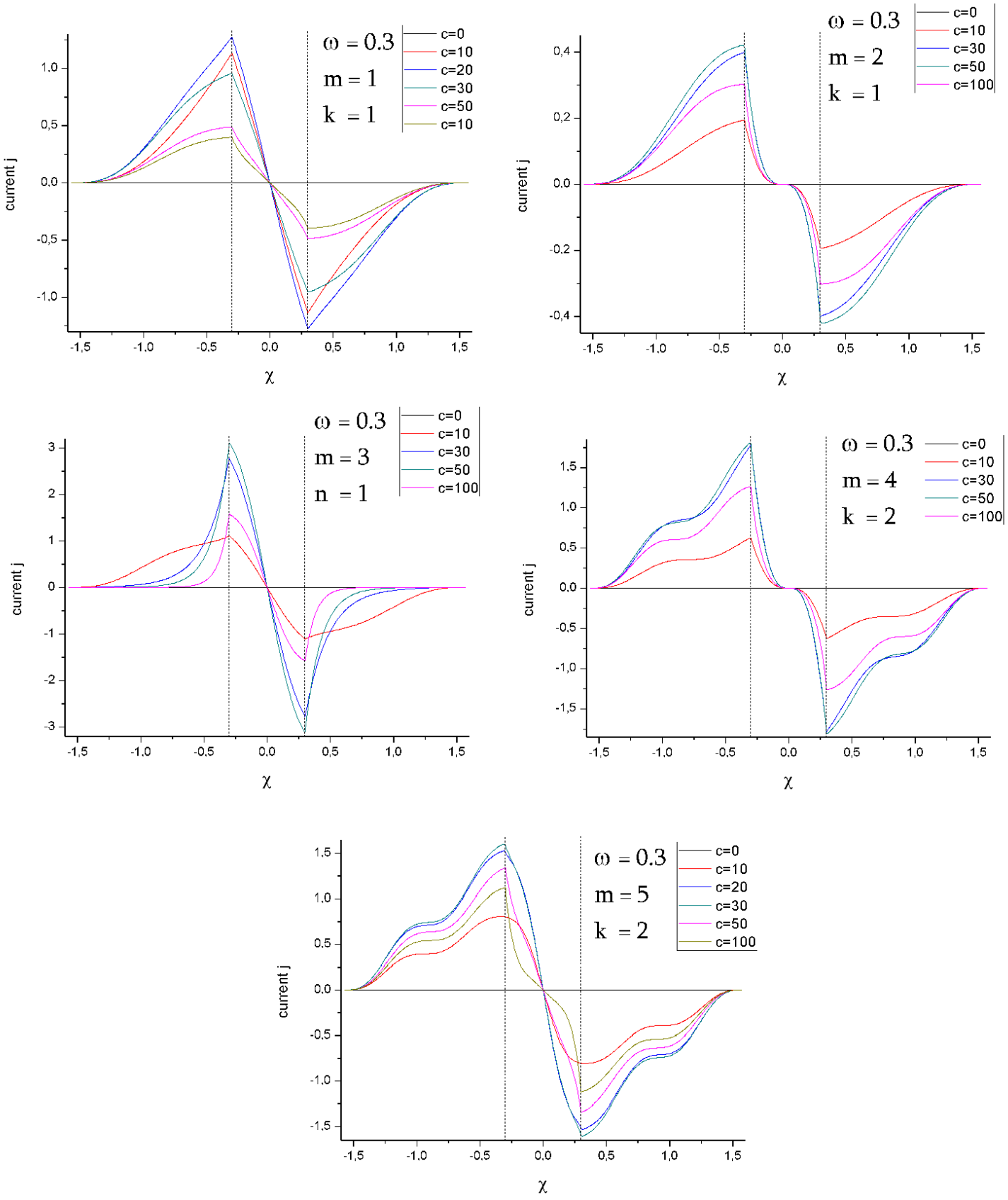

Figure 13: Currents of the lowest energies for $\omega = 0.3$ for some values of c, where ε_0–states are counted by k and ε_∞–states by n. One can see that the current is always directed to the center of the whole system. Moreover, it vanishes both for $c = 0$ and for $c \to \infty$ and is not differntiable at $\chi = \pm\omega$. Thus it reaches a maximum for some c.

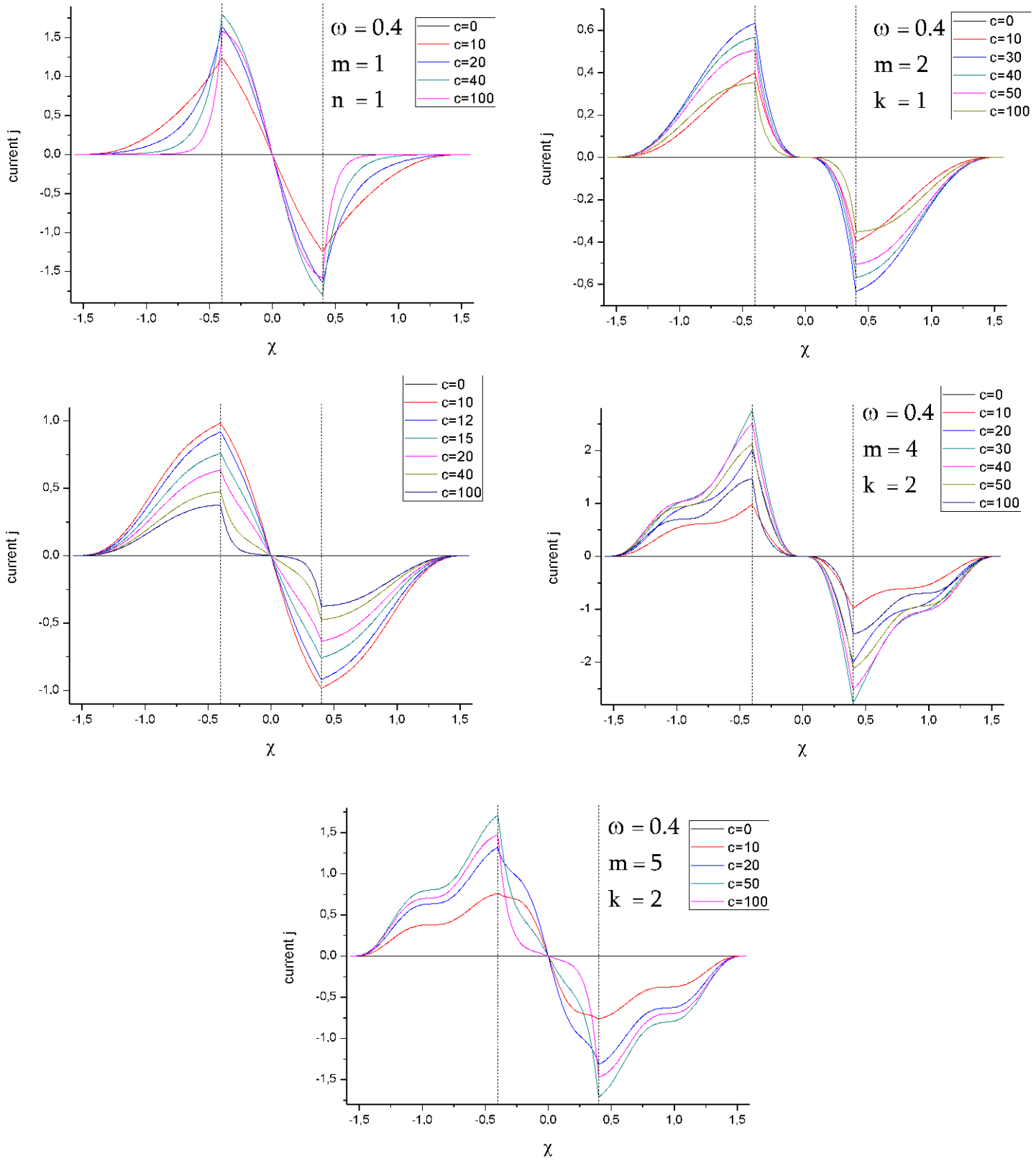

Figure 14: Currents of the lowest energies for $\omega = 0.4$ for some values of c, where ε_0–states are counted by k and ε_∞–states by n. One can see that the current is always directed to the center of the whole system. Moreover, it vanishes both for $c = 0$ and for $c \to \infty$ and is not differntiable at $\chi = \pm\omega$. Thus it reaches a maximum for some c.

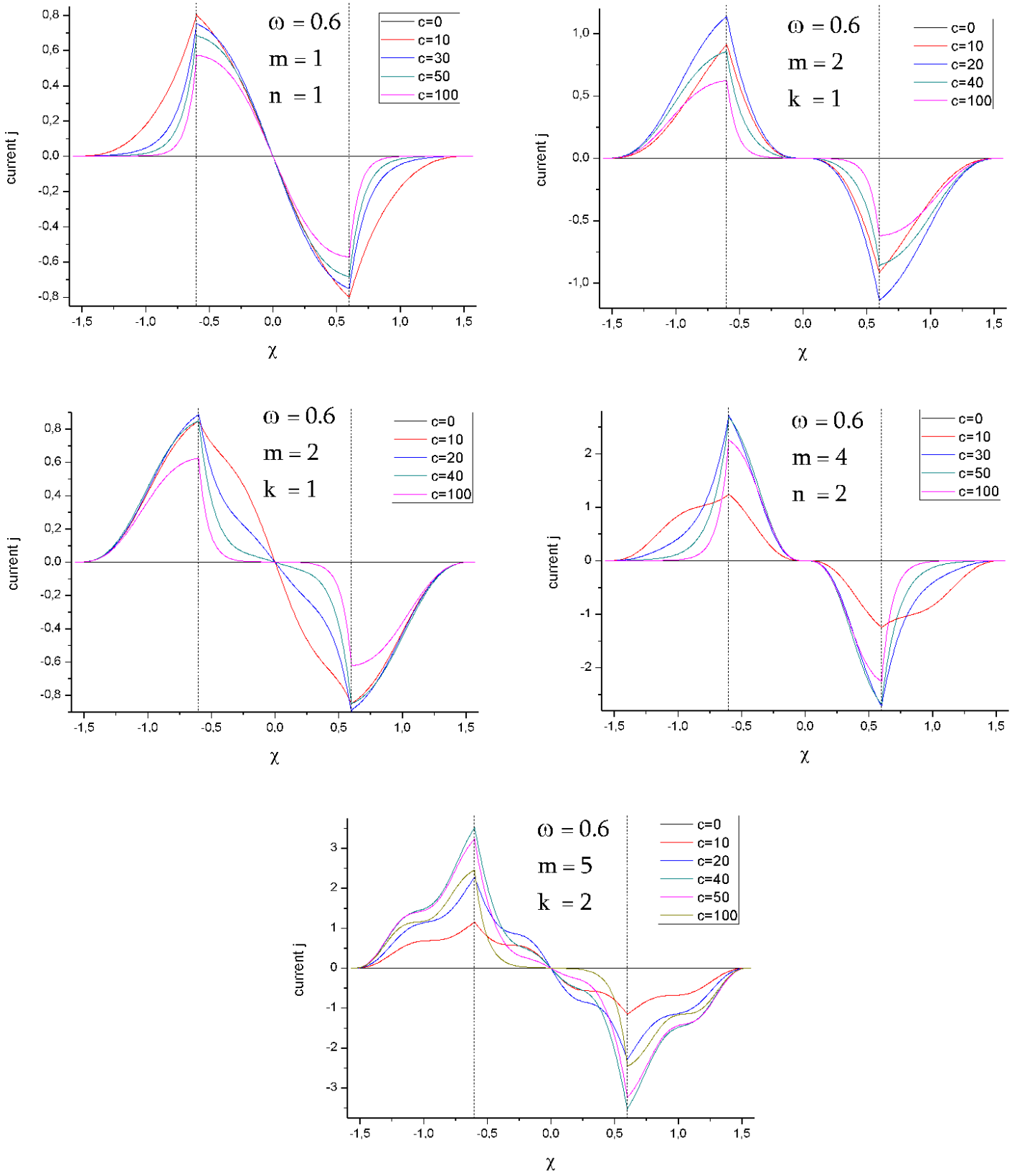

Figure 15: Currents of the lowest energies for $\omega = 0.6$ for some values of c, where ε_0–states are counted by k and ε_∞–states by n. One can see that the current is always directed to the center of the whole system. Moreover, it vanishes both for $c = 0$ and for $c \to \infty$ and is not differntiable at $\chi = \pm\omega$. Thus it reaches a maximum for some c.

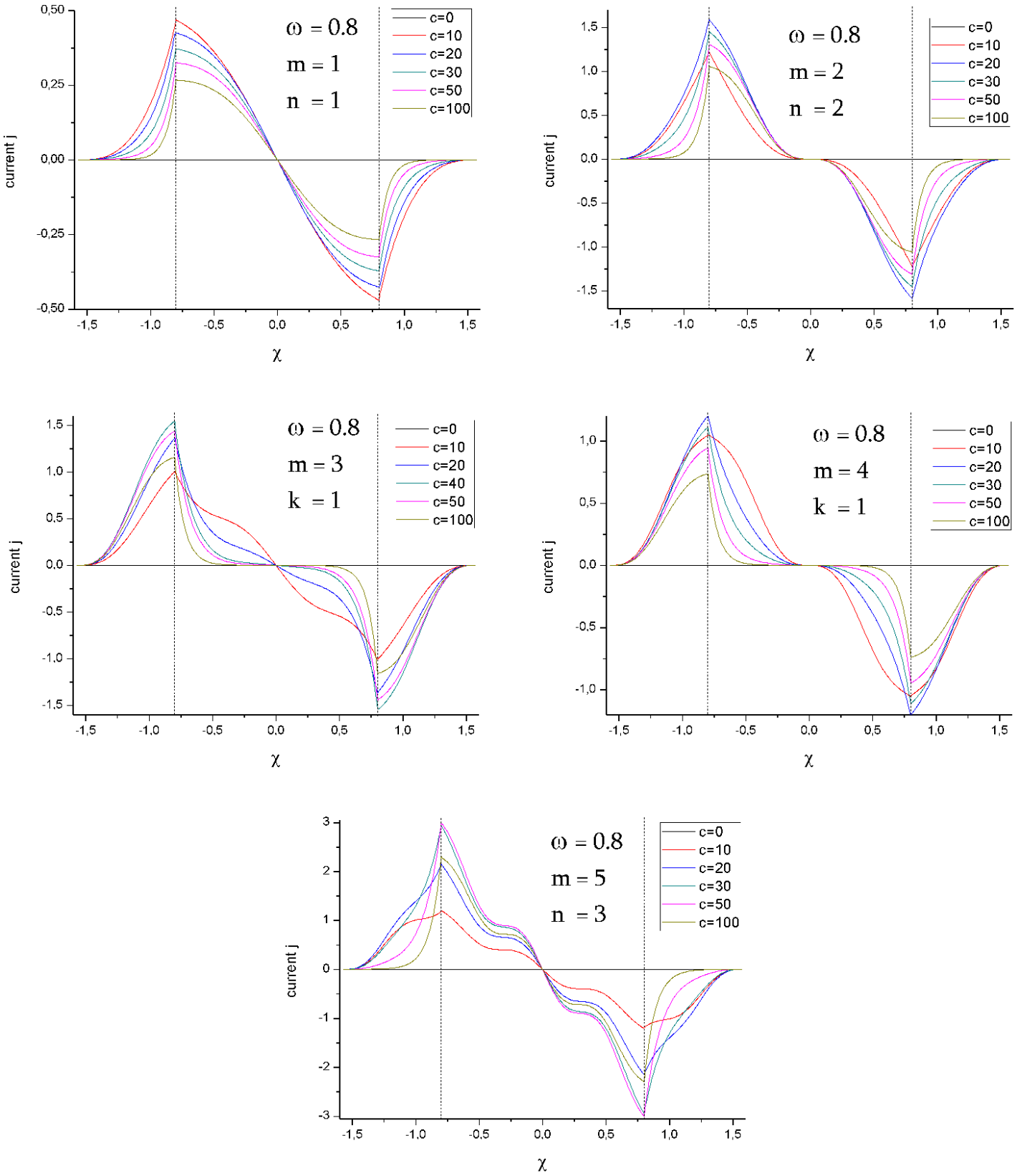

Figure 16: Currents of the lowest energies for $\omega = 0.8$ for some values of c, where ε_0–states are counted by k and ε_∞–states by n. One can see that the current is always directed to the center of the whole system. Moreover, it vanishes both for $c = 0$ and for $c \to \infty$ and is not differntiable at $\chi = \pm\omega$. Thus it reaches a maximum for some c.

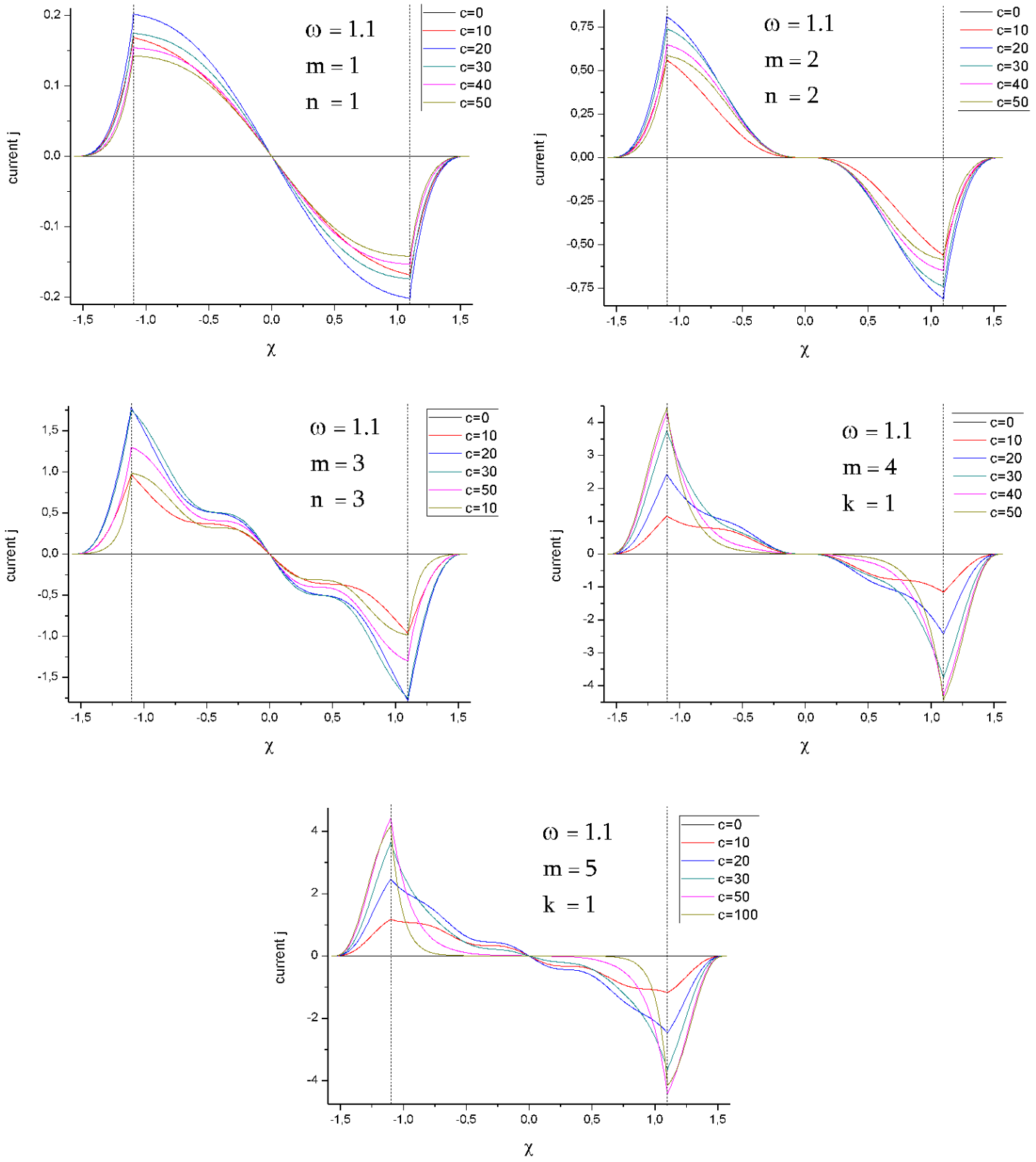

Figure 17: Currents of the lowest energies for $\omega = 1.1$ for some values of c, where ε_0–states are counted by k and ε_∞–states by n. One can see that the current is always directed to the center of the whole system. Moreover, it vanishes both for $c = 0$ and for $c \to \infty$ and is not differntiable at $\chi = \pm\omega$. Thus it reaches a maximum for some c.

3.4.2 Discussion

First we can confirm that for $c = 0$ the probability current vanishes. For increasing perturbation the current rises, too, until it reaches a maximum, which seems to depend on the particular waist and the type of the respective state. Furthermore, one can observe that the current is an antisymmetric function which is not differentiable at $\chi = \pm\omega$ as we already found out in the discussion of the continuity equation in Section 2.2. Generally one can state that the current is always directed towards the center of the potential well, that is the probability "flows" into the center where the imaginary potential describes a particle loss. Note that positive currents stand for positive χ-direction while negative ones yield the opposite direction. Another issue, that catches the eye, is that for increasing c the current decreases after it reached its maximum. This looks plausible as we know from the discussion of the densities that for $c \to \infty$ three separated potential wells emerge so that the current has to vanish for each of them since we already found out that for the familiar potential well the current is equal to zero. Another observation is the distinct behaviour for ε_0–states on the one hand and ε_∞–states on the other hand. For ε_0–states the current first thins out in area 2, that is in the inner region the current decreases already for small c in a very strong way which is getting stronger for increasing c. Otherwise for ε_∞–states we find exactly the inverse situation. In this case the current rapidly increases in the outer region while the decay in area 2 is quite flat. Furthermore, ε_0–states reach their maximum for smaller c than ε_∞–states as we can read off from the graphs. Moreover, one can see a kind of plateau for the currents of some states. These occur especially for higher states, that is for states with a higher value of m. But only in one region, inner or outer, the plateau endures for increasing c, that is this one, where the current does not decrease more and more rapidly for increasing perturbation.

All in all we can state that the current is always directed towards the center of the well. An interpretation of this could be that in the center there is a drain of probability, which is followed by a current towards it. We already discussed this in Section 2.3 and concluded from the continuity equation that there has to occur a drain in the center. For ε_0–states the current increases in area 1 and 3 and has a maximum at $\chi = \pm\omega$. Then it decreases strongly so that for $c \gg 1$ there is actually no current any more far beyond the borderlines of the areas. We already know from the discussion of the densities that this kind of state thins out in the center of the well for increasing c. Also the maximum becomes lower so that for $c \to \infty$ there is no current any more. The situation for ε_∞–states is vice verca. For increasing c the decay of the current goes up in area 1 and 2 and keeps comparatively flat in area 2. From Section 3.3 we know that the ε_∞–states vanish in the outer region for increasing c.
Maybe the most interesting fact is that there occurs a maximum for some finite c, which seems to be logical because the current has to vanish for $c \to \infty$ and $c \to 0$. This special value of perturbation maybe has a special relevance that should be investigated in more detail. In this context one should interpret also the occuring plateaus in the currents for higher states.

4 Outlook

Finally we present some possibilities for further studies of this topic since there remains a lot to proceed that would have gone beyond the scope of this research training work.

4.1 Time evolution and interpretation of imaginary energies

Already in the discussion of the Schrödinger equation we found out that the imaginary potential leads to a non-vanishing imaginary part of the energy but after all we still do not know its effect apart from its influence on the time evolution. We only saw that it seems to characterize and to divide the states into two groups where for the one group it tends to zero so that a familiar potential well is formed and for the other group it approaches $-c$ and a kind of familiar potential well in the center is formed as well. The only difference is that the imaginary part of the energy indicates the depth of the well.
One has to study in more detail the time evolution of the system which is governed by E_I and find out in what way it influences the system and whether it is reasonable to talk about arising potential wells for $c \to \infty$ at all since this stands for an extremely strong damping of the system. The interesting issue is that only ε_∞–states are damped that strong while the damping of the ε_0–states decreases for increasing perturbation c. This could directly be seen by evaluating the time evolution operator

$$U\left(t-t_0\right) = \exp\left[-\frac{i}{\hbar}E(t-t_0)\right] = \exp\left[-\frac{i}{\hbar}E_R(t-t_0)\right]\exp\left[\frac{1}{\hbar}E_I(t-t_0)\right]. \tag{4.1}$$

The first factor is only a phase factor which does not have any physical impact since it drops out for the densities. The second factor yields an exponential decay since the argument is real and, as we found out in Section 2.2, is always negative for positive times. From the behaviour of E_I we can conclude this distinct time evolution.
This insight has a quite central character for the whole model of a complex potential since we intend to model the perturbation as a kind of dissipation. As we found out in Section 2.1 and Eq. (2.9) the damping of the density decreases with E_I. Since ε_0–states, where $\lim_{c\to\infty}\varepsilon_{I,0} = 0$, are shifted to area 1 and 3 and ε_∞–states, where $\lim_{c\to\infty}\varepsilon_{I,\infty} = -\lim_{c\to\infty} c$, to area 2 the damping increases in the center of the well and vanishes in the outer regions for large c. The result for a quite strong perturbation $c \gg 1$ is then a dip in the center of the density which maintains the interpretation of dissipation.

4.2 Determination of critical waist

Another improvement would certainly be to find a more backed agreement for ω_{crit}, that is the waist where a ε_0–state and a ε_∞–state change roles. This could provide a deeper insight how both states are mixed for a general waist $\omega \in (0, \pi/2)$. Maybe we were on a good way in Subsection 3.3.2 so that a possible approach to achieve this could be a further evaluation of the graphs of the densities and the energies, that is a deeper discussion of the occuring and vanishing maxima and minima of the densities as well as a closer look, for example, on the imaginary part of the energy. We can see from Figs. 3 and 4 that while the ε_∞–states have a slight buckle for some c the ε_0–states

show a minimum there. These peculiarities occur at some c, which slowly grows with ω and m and they are especially strong just for $\omega \approx \omega_{\text{crit}}$. Hence there could be a connection between both effects. Furthermore, it would be interesting to determine the particular perturbation c where these effects are occuring because until this c the states continuously become the calculated limits of two seperated potential wells. For $c = 0$ there are only the familiar states of the real potential well. The increasing perturbation provides a mixing of these "old" ε_0–states with the "new" ε_∞–states until some c after that the states untangle into the two respective groups. Thus another improvement could be to evaluate this particular perturbation c and understand its physical background.

4.3 More accurate derivation of real part of energy

In Subsection 3.2.1 we computed the limit of the real part of the energy for $c \to \infty$ and got some reasonable results. Nevertheless the imaginary part of (3.32) yields the contradiction $\lim_{c\to\infty} c = 0$. A more accurate approximation of the imaginary part of the energy than the linear or the constant one, respectively, could eliminate this weak point. This incorrectness obviously arises from the choice of the approximation. The next step to make this more accurate could be an exponential or a polynomial fit of the deviation of this approximation that is $\varepsilon_{I,\infty} + c$ and $\varepsilon_{I,0}$ since we only took the leading limits $\varepsilon_{I,\infty} \approx -c$ and $\varepsilon_{I,0} \approx 0$ into account.

4.4 Further discussion of densities and currents

There are still a couple of things to have a deeper look at. The most obvious one is definitely an extensive discussion of the maxima occuring in the graphs of the current in Section 3.4, that is the value of the maxima, the particular perturbation c it occurs for, the quantities it depends on as well as the physical interpretation of it. Furthermore, the calculation of the limits $c \to \infty$ for ρ and j would provide some interesting insights and we could try to prove that $\lim_{c\to\infty} j = 0$ holds as it should be and whether the maximum always occurs at $\chi = \pm\omega$ as well as get a theoretical device of the separated potential wells we only found graphically. Another possibility to improve this work could be a serious interpretation of the current at $\chi = \pm\omega$ that is the occuring maxima as well as the non-differentiability of j right there.

4.5 Evaluation of higher states

Another obviously time consuming and quite tedious extension could also be the evaluation of higher states than $m = 5$. This should at least provide some helpful suggestions how to calculate ω_{crit} since we do not know if the formula in Subsection 3.3.2 is correct because we have no other examples to compare with. Moreover, it allows a further look at the development of energy, density and current, which could be useful to see the whole picture.

4.6 More general approach

In the whole work we restricted ourselves to the one-dimensional Schrödinger equation. The next step would be to generalize this to more spatial dimensions and take interactions into account that would lead to a nonlinear Schrödinger equation, which is the Gross-Pitaevskii equation (1.2).

Furthermore, the potential has been chosen quite simple so that it is possible to extend this to a harmonic one to model the Gaussian electron beam as a perturbation of the system in a more accurate way.

References

[1] S. N. Bose, *Plancks Gesetz und Lichtquantenhypothese*, Z. Phys. **26**, 178 (1924)

[2] A. Einstein, *Quantentheorie des einatomigen idealen Gases - Zweite Abhandlung*, Sitz. Ber. Preuss. Akad. Wiss. (Berlin) **22**, 261 (1924)

[3] M. H. Anderson, J. R. Ensher, M. R. Matthews, C. E. Wieman, and E. A. Cornell, *Observation of a Bose-Einstein Condensation in a Dilute Atomic Varpor*, Science **269**, 198 (1995)

[4] K. B. Davis, M. O. Mewes, M. R. Andrews, N. J. van Druten, D. S. Durfee, D. D. Kurn, and W. Ketterle, *Bose-Einstein Condensation in a Gas of Sodium Atoms*, Phys. Rev. Lett. **75**, 3969 (1995)

[5] W. D. Phillips and H. J. Metcalf, *Cooling and Trapping Atoms*, Scientific American **256**, 36 (1987)

[6] C. N. Cohen-Tannoudji and W.D. Phillips, *New Mechanism for Laser Cooling*, Physics Today, 33 (1990)

[7] S. Chu, *Laser Trapping of Neutral Particles*, Scientific American **266**, 71 (1992)

[8] W. Ketterle and N. J. van Druten, *Evaporative Cooling of trapped atoms*, Adv. Atom. Mol. Phys. **37**, 181 (1996)

[9] M. R. Andrews, C. G. Townsend, H.-J. Miesner, D. S. Durfee, D. M. Kurn, and W. Ketterle, *Observation of interference between two Bose condensates*, Science **275**, 637 (1997)

[10] C. Orzel, A. K. Tuchman, M. L. Fenselau, M. Yasuda, and M. A. Kasevich, *Squeezed States in a Bose-Einstein Condensate*, Science **291**, 2386 (2001)

[11] M. Greiner, O. Mandel, T. Esslinger, T. W. Hänsch, and I. Bloch, *Quantum phase transition from a superfluid to a Mott insulator in a gas of ultracold atoms*, Nature **415**, 39 (2002)

[12] I. Bloch, *Quantum coherence and entanglement with ultracold atoms in optical lattices*, Nature **453**, 1016 (2008)

[13] J. E. Lye, L. Fallani, M. Modugno, D. S. Wiersma, C. Fort, and M. Inguscio, *Bose-Einstein Condensation in a Random Potential*, Phys. Rev. Lett. **95**, 070401, (2005).

[14] J. Bardeen, L. N. Cooper, and J. R. Schrieffer, *Theory of Superconductivity*, Phys. Rev. **108**, 1175 (1957)

[15] L. Salasnich, N. Manini, and A. Parola, *Condensate Fraction of a Fermi Gas in the BCS-BEC Crossover*, Phys. Rev. A **72**, 023621 (2005)

[16] P. Würtz, T. Langen, T. Gericke, A. Koglbauer, and H. Ott, *Experimental Demonstration of Single-Site Addressability in a Two-Dimensional Optical Lattice*, Phys. Rev. Lett. **103**, 080404 (2009)

[17] T. Gericke, P. Würtz, D. Reitz, T. Langen, and H. Ott, *High-resolution scanning electron microscopy of an ultracold quantum gas*, Nature Phys. **4**, 949 (2008)

[18] S. Schmid, A. Härter, and J. H. Denschlag, *Dynamics of a Cold Trapped Ion in a Bose-Einstein Condensate*, Phys. Rev. Lett. **105**, 133202 (2010)

[19] K. D. Nelson, X. Li, and D. S. Weiss, *Imaging single atoms in a three-dimensional array*, Nature Phys. **3**, 556 (2007)

[20] N. Gemelke, X. Zhang, C.-L. Hung, and C. Chin, *In situ oservation of incrompressible Mott-insulating domains in ultracold atomic gases*, Nature **460**, 995 (2009)

[21] M. Karski, L. Förster, J. M. Choi, W. Alt, A. Widera, and D. Meschede, *Nearest-neighbor detection of atoms in a 1D optical lattice by fluorescence imaging*, Phys. Rev. Lett. **102**, 053001 (2009)

[22] W. S. Bakr, J. I. Gillen, A. Peng, S. Fölling, and M. Greiner, *A quantum gas microscope for detecting single atoms in a Hubbard regime optical lattice*, Nature **462**, 74 (2009)

[23] A. Marte, *Feshbach-Resonanzen bei Stößen ultrakalter Rubidiumatome*, PhD Thesis, Technical University of Munich (2003), `http://mediatum2.ub.tum.de/doc/602987/602987.pdf`

[24] C. J. Pethick and H. Smith, *Bose-Einstein Condensation in Dilute Gases*, 2nd Edition, Cambridge University Press, 2008

[25] W. Nolting, *Grundkurs Theoretische Physik 5/1, Quantenmechanik - Grundlagen*, 6th Edition, Springer, 2001

[26] W. Nolting, *Grundkurs Theoretische Physik 5/2, Quantenmechanik - Methoden und Anwendungen*, 6th Edition, Springer, 2007

[27] F. Schwabl, *Quantenmechanik (QM I)*, 6th Edition, Springer, 2002